Supplementary Figure 1. Caspase-4/11 is required for *Alu*-induced RPE degeneration.

(**a**) Protein lysates from RPE of human donor eyes were immunoblotted with an isotype antibody (control for anti-caspase-4 immunoblotting antibody in Figure 1a). No immunoreactive bands were observed in isotype control immunoblot. (**b**) Human RPE cells mock treated or stimulated with *Alu* RNA. Protein lysates were immunoblotted with secondary antibody alone, an isotype antibody, or an anti-caspase-4 antibody; pro-caspase-4 and p30 cleavage product of caspase-4 activation (Casp4 p30) were observed in *Alu* RNA stimulated cells; no bands were observed in secondary alone or isotype control immunoblots. Specific bands of interest are indicated by arrowheads. (**c**) Relative abundance of CASP4 mRNA in human RPE cells mock-transfected or transfected with *Alu* RNA. Data presented are mean ± SEM; $n = 3$ independent experiments; $^{*}P = 0.0007$, two-tailed t test. (**d**) Immunoblot for pro-caspase-4 (pro-casp4) and p30 cleavage product of caspase-4 (Casp4 p30) in human RPE cells transfected with DICER1 or control (Ctr) anti-sense oligonucleotides (AS) along with simultaneous transfection of *Alu* RNA antisense oligonucleotides (*Alu* AS) or scrambled oligonucleotide (Scr). (**e**) Immunoblot for pro-caspase-11 (procasp-11) and p30 cleavage product of caspase-11 (Casp11 p30) in WT mouse RPE cells mock transfected or transfected with *Alu* RNA, or Alu expression plasmid (pAlu) or empty vector control (pNull). (**f**) Fundus photographs and immunofluorescence staining of zonula occludens-1 (ZO-1) on RPE flat mounts of the *WT* (n = 6 eyes) and *Casp11*$^{-/-}$ (n = 10 eyes) mice subretinally injected with empty vector control (pNull) or *Alu* expression plasmid (pAlu). (**g**) Fundus photographs and immunofluorescence staining of zonula occludens-1 (ZO-1) on RPE flat mounts of 129S6 mice which carry a caspase-11 inactivating passenger mutation subretinally injected (n = 7 eyes) with vehicle or *Alu* RNA, or injected with (n = 5 eyes) *Alu* expression plasmid or empty vector control. (**h**) Fundus photographs and immunofluorescence staining of zonula occludens-1 (ZO-1) on RPE

flat mounts of WT (n = 7 eyes) and 129S6 (n = 10 eyes) mice, which carry a caspase-11 inactivating passenger mutation, subretinally injected with control siRNA or DICER1 targeted siRNA. For all immunoblots, cropped gel image of bands of interest of representative immunoblots of three independent experiments and densitometric analysis (mean (SEM)) are shown. In **g** and **h**, binary (Healthy %) and morphometric (PM, polymegethism (mean (SEM)) quantification of RPE degeneration are shown (two-tailed t test; **P* < 0.05; ***P* < 0.01; ****P* < 0.001). Loss of regular hexagonal cellular boundaries in ZO-1 stained flat mounts is indicative of degenerated RPE. The degenerated retinal area is outlined by blue arrowheads in the fundus images.

Supplementary Figure 2. **Caspase-11 is required for *Alu* RNA-induced caspase-1 activation and RPE degeneration.**

(**a**) Caspase-1 activity levels in *Alu* RNA transfected *Casp11*$^{-/-}$ mouse RPE cells reconstituted via transfection of caspase-11 expression plasmid (pcasp11; n = 5 randomly chosen microscopic fields) or control plasmid (pNull; n = 7 randomly chosen microscopic fields). Caspase-1 activity was assessed using CaspaLux®1-E_1D_2. **P* = 0.0001, two-tailed t test; error bars denote SEM. (**b**) Immunoblot for pro-caspase-1 (procasp-11) and p10 cleavage product of caspase-1 (Casp1 p10) in mock-transfected or *Alu* RNA transfected *Casp11*$^{-/-}$ mouse RPE cells that had been transfected with empty vector plasmid (vector) or Caspase-11 expression plasmid (pCasp11). (**c**) Fundus photographs and immunofluorescence staining of zonula occludens-1 (ZO-1) on RPE flat mounts of the WT (n = 6 eyes) or caspase-1 and caspase-11 deficient mice (*Casp1*$^{-/-}$ *Casp11*$^{129mt/129mt}$; n = 6 eyes) or *Casp1*$^{-/-}$ *Casp11*$^{129mt/129mt}$ mice expressing functional mouse caspase-11 from a bacterial artificial chromosome transgene (*Casp1*$^{-/-}$ *Casp11*$^{129mt/129mt}$ *Casp11*^{Tg}; n = 5 eyes), subretinally injected with *Alu* expression plasmid (pAlu) or empty vector control (pNull). (**d**,**e**) Immunoblot

for pro-caspase-11 (procasp-11) and p30 cleavage product of caspase-11 (Casp11 p30) in mock-transfected or *Alu* RNA transfected (**d**) WT and *P2rx7*$^{-/-}$ mouse RPE cells (**e**) WT and *Pycard*$^{-/-}$ mouse RPE cells. For all immunoblots, cropped gel image of bands of interest of representative immunoblots of three independent experiments and densitometric analysis (mean (SEM)) are shown. In **c**, binary (Healthy %) and morphometric (PM, polymegethism (mean (SEM)) quantification of RPE degeneration are shown (two-tailed t test; **P* < 0.05; ***P* < 0.01; ****P* < 0.001). Loss of regular hexagonal cellular boundaries in ZO-1 stained flat mounts is indicative of degenerated RPE. The degenerated retinal area is outlined by blue arrowheads in the fundus images.

Supplementary Figure 3. Cellular morphometry analysis. Quantification of mean cell size, cell density, and cell size variability obtained by analyzing zonula occludens-1 (ZO-1) immunofluorescence staining of RPE flat mounts from wild-type mice. The analyses were performed in semi-automated fashion by 3 masked raters. For all panels, Vehicle (n = 16 eyes); *Alu* RNA (n = 30 eyes); pNull (n = 14 eyes); pAlu (n = 20 eyes). ****P* < 0.0001, two-tailed t test. Box plot shows median (red line), interquartile range (box), and the extremes (line segments).

Supplementary Figure 4. Increased abundance of phospholipid oxidation products in *Alu* RNA-stimulated RPE cells.

(**a**) Brief schematic highlighting select products of PAPC (1-palmitoyl-2-arachidonyl-sn-glycero-3-phosphocholine) oxidation, collectively referred to as oxPAPC.

(**b**) Representative mass scan of pure unoxidized PAPC and oxPAPC using an ABI Sciex 4000 QTrap mass spectrometer.

(**c**) Representative mass scan of oxPAPC, formed from air-oxidized PAPC.

(**d**) Quantification of individual species of oxPAPC by liquid chromatography-mass spectrometry. Human RPE cells stimulated with *Alu* RNA had higher levels of PGPC (1-palmitoyl-2-glutaroyl-sn-glycero-3-phosphocholine) and LysoPC (1-palmitoyl-2-hydroxy-sn-glycero-3-phosphocholine) levels, indicative of extended oxidation, concomitant with a trending decrease of precursor PAPC and intermediate POVPC. $n = 6$ cell culture replicates; * $P < 0.05$, two-tailed t test; error bars denote standard error.

Supplementary Figure 5. Gasdermin D is required for *Alu*-induced RPE degeneration.

(**a**) Fundus photographs and immunofluorescence staining of zonula occludens-1 (ZO-1) on RPE flat mounts of the WT (n = 7 eyes) and *Gsdmd*$^{-/-}$ (n = 9 eyes) mice subretinally injected with *Alu* expression plasmid (pAlu) or empty vector control plasmid (pNull). (**b**) Fundus photographs and immunofluorescence staining of zonula occludens-1 (ZO-1) on RPE flat mounts of the WT (n = 6 eyes) and *Gsdmd*$^{-/-}$ (n = 10 eyes) mice subretinally injected with control siRNA or siDICER1. (**c**) Secretion of IL-18 by mock-transfected or *Alu* RNA transfected *Gsdmd*$^{-/-}$ mouse RPE cells that had been reconstituted via transfection of expression plasmid for wild type GSDMD (pGSDMD-WT) or a mutant GSDMD that is uncleavable by inflammasome activation (pGSDMD-D276A) or empty vector control. Data presented are mean ± SD; n = 3 cell culture replicates; *$P = 0.02$ for empty vector vs. pGSDMD-WT *Alu* RNA transfected; *$P = 0.019$ for empty vector vs. pGSDMD-D276A *Alu* RNA transfected; two-tailed t test, error bars denote SEM. (**d**) Relative abundance of mRNA expression cytokines IL-8, IL-6, and MIP-1α in the RPE of human AMD eyes (n = 4) and healthy age-matched control eyes (n = 4); Data presented are mean ± SEM. In **a** and **b**, binary (Healthy %) and morphometric (PM, polymegethism (mean (SEM)) quantification of RPE

degeneration are shown (two-tailed t test; *$P < 0.05$; **, $P < 0.01$; ***, $P < 0.001$). Loss of regular hexagonal cellular boundaries in ZO-1 stained flat mounts is indicative of degenerated RPE. The degenerated retinal area is outlined by blue arrowheads in the fundus images.

Supplementary Figure 6. *Alu* RNA induces apoptotic cell death in human RPE cells.

Human RPE cells mock treated or stimulated with *Alu* RNA were incubated with FITC-conjugated annexin V (green) and propidium iodide (PI, red). Staining by annexin V and PI uptake was monitored by time-lapse imaging. Representative images at various time points showing annexin V and PI staining is presented for (**a**) *Alu* RNA stimulated and (**b**) mock treated human RPE cells. Representative images from three independent experiments are shown.

Supplementary Figure 7. *Alu* RNA induces apoptotic RPE cell death in mice and in human cell culture.

(**a**) Annexin V (periwinkle blue) and propidium iodide (PI; red) staining of RPE flat mounts from WT mice subretinbally injected with *Alu* RNA or vehicle. Row #1-2 (*Alu* RNA degenerated area): The area of *Alu* RNA-induced RPE degeneration; Row #3-4 (*Alu* RNA healthy): The RPE in regions of the eye distant from the site of *Alu* RNA exposure; Row #5 (*Alu* RNA unstained): The area of *Alu* RNA-induced RPE degeneration that was not stained; Row #6-7 (PBS): The area of mouse eye subretinal injected with vehicle control. ON, optic nerve. Representative images from n = 8 eyes per group are shown. (**b**) Immunoblots of cleaved caspase-3 and cleaved PARP1 in human RPE cells either mock-transfected or transfected with *Alu* RNA. For all immunoblots, cropped gel image of bands of interest of representative immunoblots of three independent experiments and densitometric analysis (mean (SEM)) are shown.

Supplementary Figure 8. Resistance of the RPE in *Gsdmd*$^{-/-}$ mice to *Alu* RNA-induced apoptotic cell death is overcome by IL-18.

Annexin V (periwinkle blue) and propidium iodide (PI; red) staining of RPE flat mounts of *Gsdmd*$^{-/-}$ mice subretinally injected with *Alu* RNA or *Alu* RNA plus recombinant mouse IL-18 (Alu RNA+recIL-18). ON, optic nerve. Representative images from n = 8 eyes are shown.

Supplementary Figure 9. Interferon signaling in RPE toxicity.

(**a**) Immunoblot of phosphorylated and total IRF3 and STAT2 in human RPE cells transfected with *Alu* RNA or mock transfected. (**b**) Immunoblot of phosphorylated and total STAT2 in WT and *Ifnar1*$^{-/-}$ mouse RPE cells transfected with *Alu* expression plasmid (pAlu) or empty vector control (pNull). (**c**) Fundus photographs and immunofluorescence staining of zonula occludens-1 (ZO-1) on RPE flat mounts of the *WT* (n = 7 eyes) and *Stat2*$^{-/-}$ (n = 7 eyes) mice subretinally injected with control siRNA or Dicer1 targeted siRNA (siDICER). (**d**) Fundus photographs and immunofluorescence staining of zonula occludens-1 (ZO-1) on RPE flat mounts of the *WT* (n = 6 eyes) and *Stat2*$^{-/-}$ (n = 7 eyes) mice subretinally injected with vehicle control or *Alu* RNA. (**e**) Immunoblot of pro-caspase-11 (pro-casp11) and p30 cleaved product of caspase-11 (p30) in WT and *Stat2*$^{-/-}$ mouse RPE cells transfected with *Alu* RNA or mock transfected. For all immunoblots, cropped gel image of bands of interest of representative immunoblots of three independent experiments and densitometric analysis (mean (SEM)) are shown. In **c** and **d**, binary (Healthy %) and morphometric (PM, polymegethism (mean (SEM)) quantification of RPE degeneration are shown (two-tailed t test; *$P < 0.05$; **$P < 0.01$; ***$P < 0.001$). Loss of regular hexagonal cellular boundaries in ZO-1 stained flat mounts is indicative of degenerated RPE. The degenerated retinal area is outlined by blue arrowheads in the fundus images.

Supplementary Figure 10. cGAS driven signaling licenses non-canonical inflammasome.

(**a**) Relative abundance of cGAS mRNA in human RPE cells mock transfected or transfected with *Alu* RNA. Data presented are mean ± SEM; n = 3 cell culture replicates; **P* = 0.006, two-tailed t test. (**b**) Immunoblot of cGAS in human RPE cells transfected with *Alu* expression plasmid (pAlu) or empty vector control (pNull) or *Alu* RNA or mock transfected (**c**) Immunoblot of pro-caspase-1 (pro-casp1) and p20 cleavage product of caspase-1 (casp1-p20) in WT and *Mb21d1*$^{-/-}$ mouse mRPE cells mock-transfected or transfected with *Alu* RNA. (**d**) Secretion of IL-18 by mouse RPE cells mock-treated or with LPS alone or LPS+ canonical inflammasome activating sodium urate (MSU) crystals. Data presented are mean ± SD; n = 3 independent experiments. (**e**) Assessment of shRNA-mediated knockdown of cGAS mRNA by RT-qPCR in human RPE cells transfected with control or DICER1 targeted antisense oligonucleotides. Representative data of three experiments presented. Data presented are mean ± SEM; n = 2 technical replicates. (**f**) Assessment of antisense oligonucleotide-mediated DICER1 mRNA knockdown by RT-qPCR in human RPE cells transduced with lentiviral vectors expressing control and cGAS targeted shRNA sequences. Representative data of three experiments presented. Data presented are mean ± SEM; n = 2 technical replicates. (**g**) Fundus photographs and immunofluorescence staining of zonula occludens-1 (ZO-1) on RPE flat mounts of the *WT* (n = 6 eyes) and *Mb21d1*$^{-/-}$ (n = 8 eyes) mice subretinally injected with empty vector plasmid control (pNull) or *Alu* expression plasmid (pAlu). (**h**) Fundus photographs and immunofluorescence staining of zonula occludens-1 (ZO-1) on RPE flat mounts of the *WT* (n = 6 eyes) and *Mb21d1*$^{-/-}$ (n = 9 eyes) mice subretinally injected with control siRNA or Dicer1 targeted siRNA (siDICER). (**i**) Relative *Ifnb* mRNA in mock or *Alu* RNA transfected *Mb21d1*$^{-/-}$ mouse RPE cells that had been reconstituted via transfection of cGAS expression plasmid (pcGAS) or empty vector plasmid. Data presented are mean ± SEM; n = 3 cell

culture replicates; *P = 0.001, two-tailed t test. For immunoblots, cropped gel image of bands of interest of representative immunoblots of three independent experiments and densitometric analysis (mean (SEM)) are shown. In **g** and **h**, binary (Healthy %) and morphometric (PM, polymegethism (mean (SEM)) quantification of RPE degeneration are shown (two-tailed t test; *P < 0.05; **P < 0.01; ***P < 0.001). Loss of regular hexagonal cellular boundaries in ZO-1 stained flat mounts is indicative of degenerated RPE. The degenerated retinal area is outlined by blue arrowheads in the fundus images.

Supplementary Figure 11. cGAS expression validation, and STING involvement in *Alu* RNA-induced IRF3 activation.

(**a**) Immunoblot of cGAS in RPE lysates from *in vitro* and *in vivo* reconstitution experiments using plasmid transfection described in Supplementary Fig. 10i and Fig. 4h, respectively. (**b**) Immunofluorescence staining of phosphorylated IRF3 (pIRF3) in wild-type and *Tmem173*$^{-/-}$ mouse RPE cells mock-transfected or transfected with *Alu* RNA. Representative images from three independent experiments are presented. (**c**) Immunoblot of phosphorylated IRF3 (pIRF3) in mock or *Alu* RNA transfected wild-type or *Tmem173*$^{-/-}$ mouse RPE cells. For immunoblots, cropped gel image of bands of interest of representative immunoblots of three independent experiments and densitometric analysis (mean (SEM)) are shown.

Supplementary Figure 12. Activation of cGAS driven signaling by *Alu* RNA is mediated by cytosolic mtDNA.

(**a**) Relative abundance of cytosolic mtDNA in human RPE cells transfected with control or DICER1 antisense (AS) oligonucleotides. Data presented are mean ± SEM; n = 3 independent experiments; data are presented as mean ± SEM ; **P* = 0.003, two-tailed t test. (**b**) Western blot shows the purity of the mitochondria-free cytosolic fractions used for measuring mtDNA abundance in cytosolic fractions; VDAC-1 is a mitochondrial marker. Representative immunoblot of three independent expreiments shown. (**c**) Relative enrichment of mtDNA in cGAS immunoprecipitate in ChIP-like pulldown assay. Mock or Poly I:C transfected indicated mouse embryonic fibroblast (MEF) were analyzed upon HA-cGAS immunoprecipitation with ant-HA antibody or isotype control. Data are presented as mean ± SEM; n = 2 cell culture replicates. (**d**) Relative enrichment of transfected plasmid DNA in cGAS immunoprecipitate in ChIP-like pulldown assay. Empty vector plasmid (puc19) transfected indicated mouse embryonic fibroblast (MEF) were analyzed upon HA-cGAS immunoprecipitation with ant-HA antibody or isotype control. Data are presented as mean ± SEM; n = 2 cell culture replicates. (**e**) Fundus photographs and immunofluorescence staining of zonula occludens-1 (ZO-1) on RPE flat mounts of WT (n = 4 eyes) and *Mb21d1*$^{-/-}$ (n = 6 eyes) mice subretinally injected with mitochondrial DNA (mtDNA). (**f**) Relative abundance of *Ifnb* mRNA in WT and *Mb21d1*$^{-/-}$ mouse RPE cells mock transfected or transfected with mitochondrial DNA (mtDNA). Data are presented as mean ± SEM; n = 3 cell culture replicates; **P* = 0.002, two-tailed t test. (**g**) Assessment of mitochondrial membrane potential (ΔΨm) using the potential-sensitive fluorochrome JC-1, in mock or *Alu* RNA transfected WT or *Ppif*$^{-/-}$ mouse RPE cells in presence or absence of cyclosporine A (CsA). Data are presented as mean ± SEM; n = 4 or 5 cell culture replicates as indicated in the figure; **P* = 0.006, two tailed

t test. (**h**) Mitochondrial permeabilization, assessed by the quenching of calcein-AM fluorescence by cobalt chloride, in mock or *Alu* RNA transfected WT or *Ppif*$^{-/-}$ mouse RPE cells in presence or absence of cyclosporine A (CsA). Data are presented as mean ± SEM; n = 3 cell culture replicates; **P* = 0.001, two tailed t test. In **e**, binary (Healthy %) and morphometric (PM, polymegethism (mean (SEM)) quantification of RPE degeneration are shown (two-tailed t test; **P* < 0.05; ***P* < 0.01; ****P* < 0.001). Loss of regular hexagonal cellular boundaries in ZO-1 stained flat mounts is indicative of degenerated RPE. The degenerated retinal area is outlined by blue arrowheads in the fundus images.

Supplementary Figure 13. Macrophages and microglia are dispensable for *Alu* RNA-induced RPE degeneration.

(**a**) Fundus photographs and immunofluorescence staining of zonula occludens-1 (ZO-1) on RPE flat mounts of WT (n = 6 eyes) mice depleted of macrophages by treatment with clodronate liposomes. (**b**) Fundus photographs and immunofluorescence staining of zonula occludens-1 (ZO-1) on RPE flat mounts of the *Cx3cr1*^{CreER} ROSA-DTA (n = 15 eyes) mice treated with tamoxifen, and subretinally injected with vehicle or *Alu* RNA. (**c**) Tamoxifen-induced depletion of microglia in *Cx3cr1*^{CreER} ROSA-DTA mice was confirmed by staining for microglial marker F4/80 superimposed with endothelial cell staining with isolectin B4 in retinal flat mounts of above mice (n = 3 mice per group). In **a** and **b**, binary (Healthy %) and morphometric (PM, polymegethism (mean (SEM)) quantification of RPE degeneration are shown (two-tailed t test; **P* < 0.05; ***P* < 0.01; ****P* < 0.001). Loss of regular hexagonal cellular boundaries in ZO-1 stained flat mounts is

indicative of degenerated RPE. The degenerated retinal area is outlined by blue arrowheads in the fundus images.

Supplementary Figure 14. Activation of caspase-1 by *Alu* RNA in bone marrow derived macrophages (BMDMs) is dependent on caspase-11, cGAS, and gasdermin D.

Immunoblots of cleaved product of caspase-1 (Casp1 p10) in mock or *Alu* RNA transfected *WT*, *Casp11*$^{-/-}$, *Mb21d1*$^{-/-}$, or *Gsdmd*$^{-/-}$ BMDMs. Representative immunoblot of three independent experiments.

Supplementary Figure 15. Model of cGAS-mediated licensing of non-canonical NLRP3 inflammasome activation by DICER deficit/*Alu* RNA. Elevated *Alu* RNA triggers release of mitochondrial DNA (mtDNA) into the cytosol. Cytosolic mtDNA subsequently activates cGAS-driven type I interferons (IFNs). The resulting IFN signaling via interferon-α/β receptor (IFNAR) and STATs triggers caspase-4/11 priming and activation that, in turn, dictates gasdermin D and NLRP3 inflammasome-mediated secretion of IL-18. Secreted IL-18 drives RPE degeneration via a mechanism involving Myd88, FAS/FasL, and caspase-8[2,22]. Three different RPE cells are depicted in the schematic model to illustrate the mechanism of *Alu* RNA–induced inflammasome activation and the autocrine and paracrine IL-18 signaling leading to RPE cell death via Myd88, Fas/FasL, Caspase-8 and Caspase-3.

Supplementary figure 1

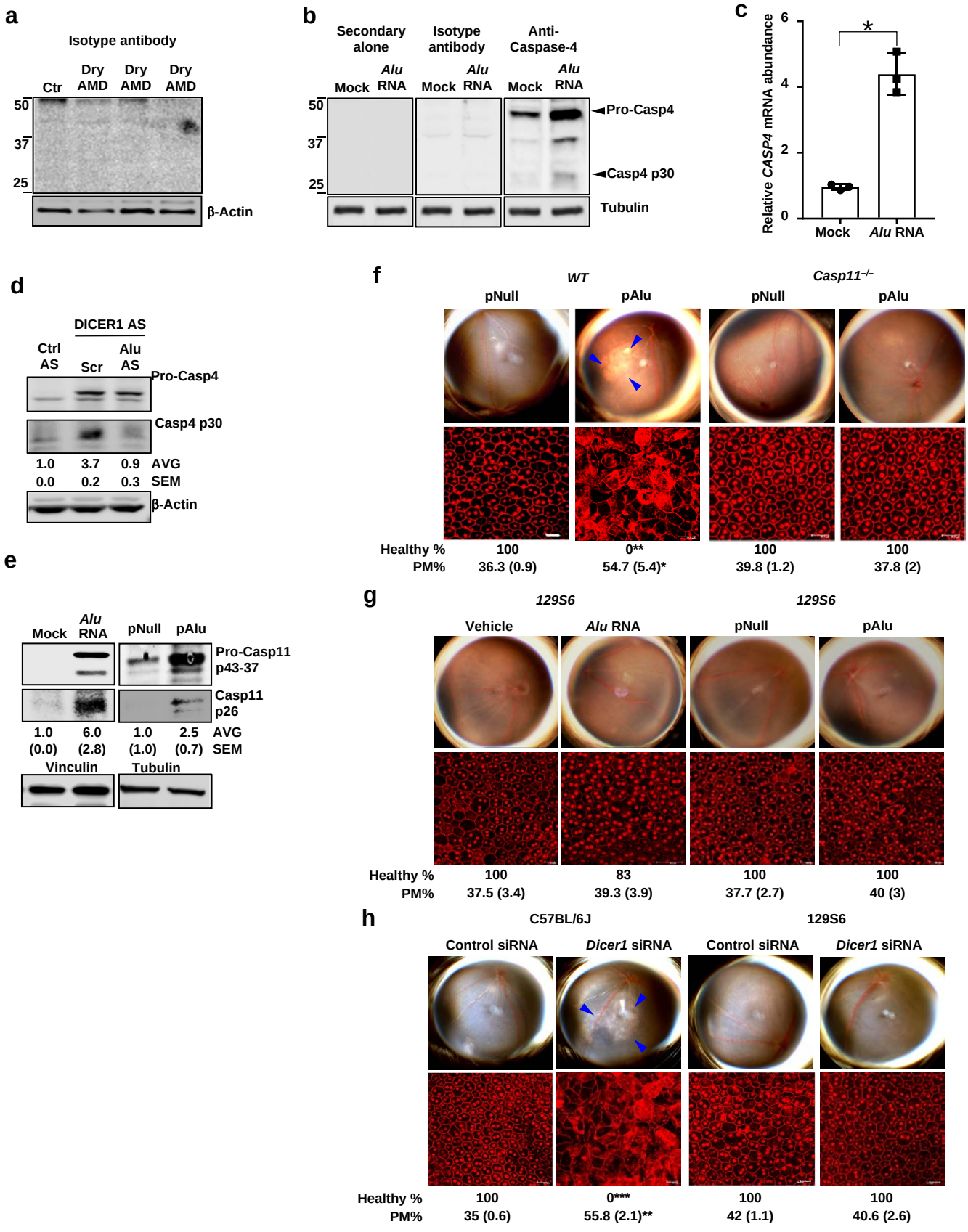

Supplementary figure 2

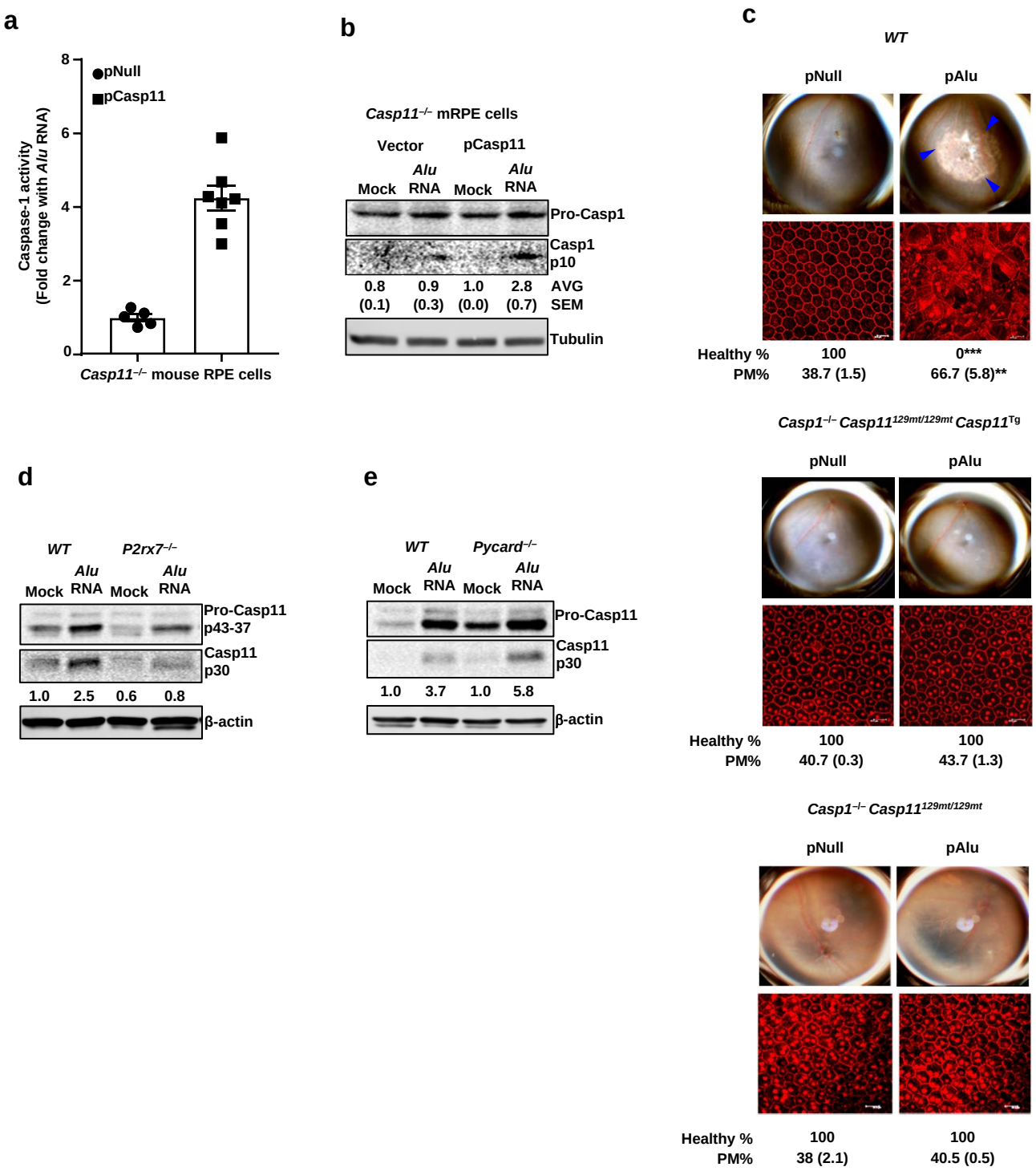

Supplementary figure 3

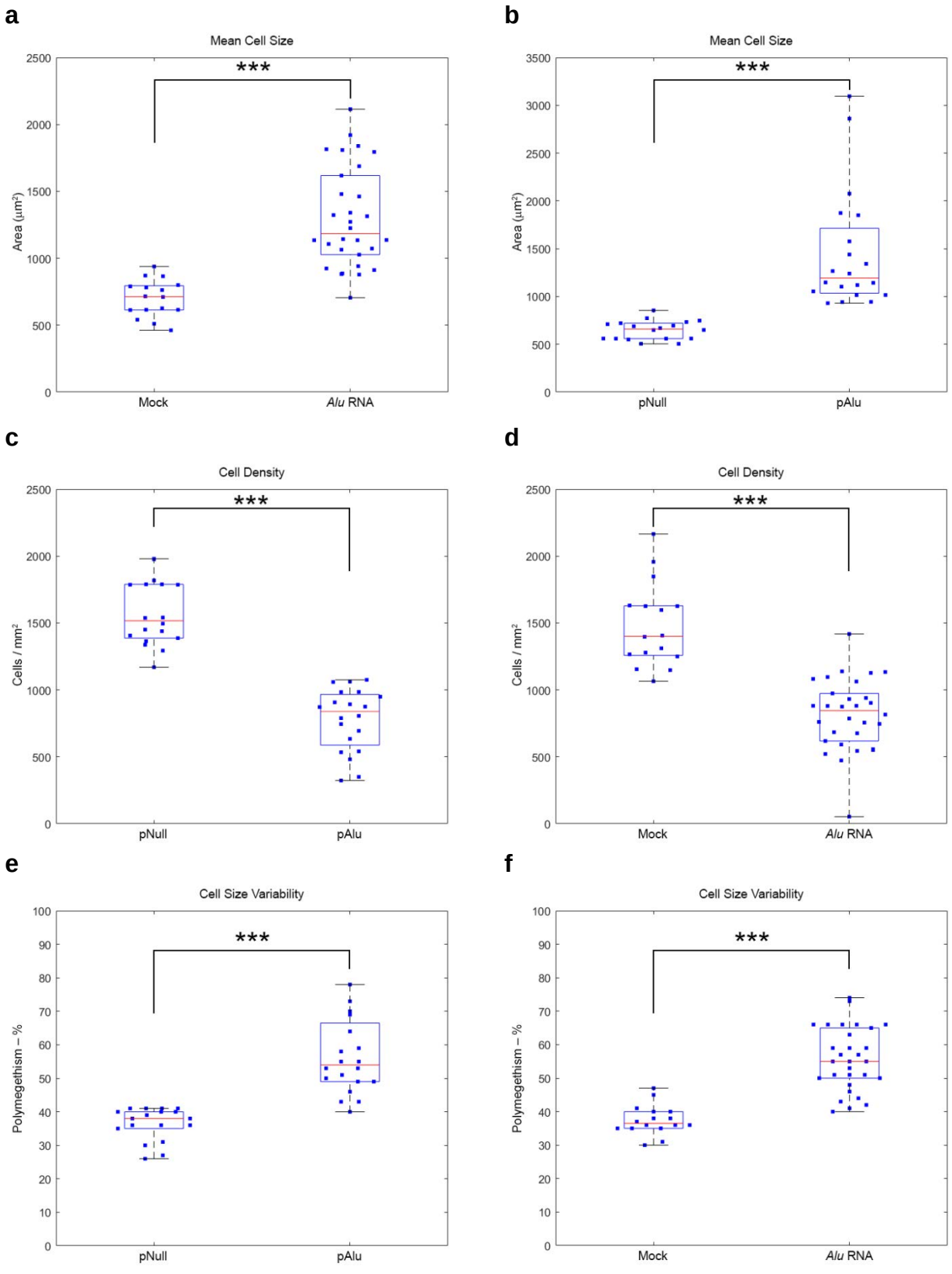

Supplementary figure 4

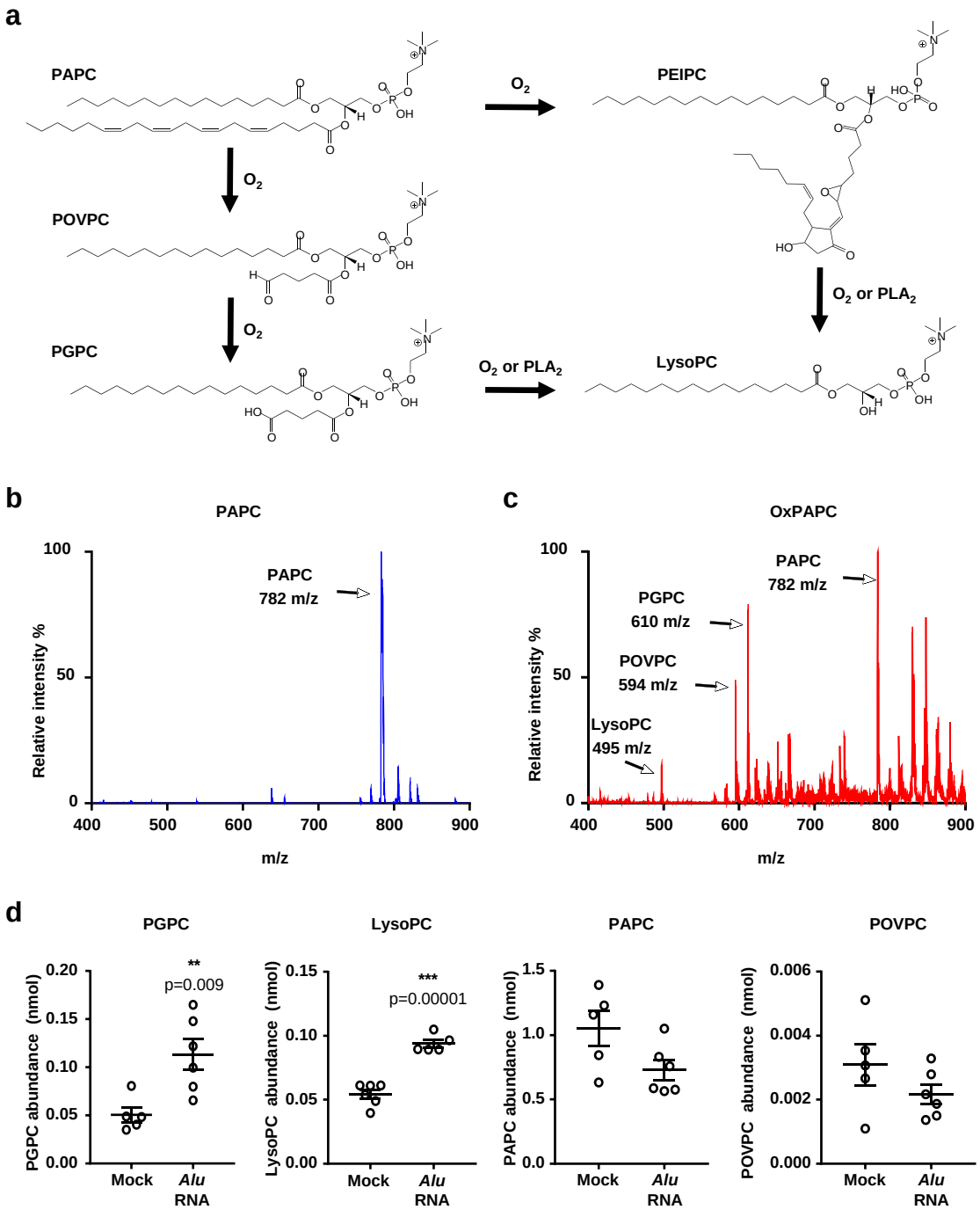

Supplementary figure 5

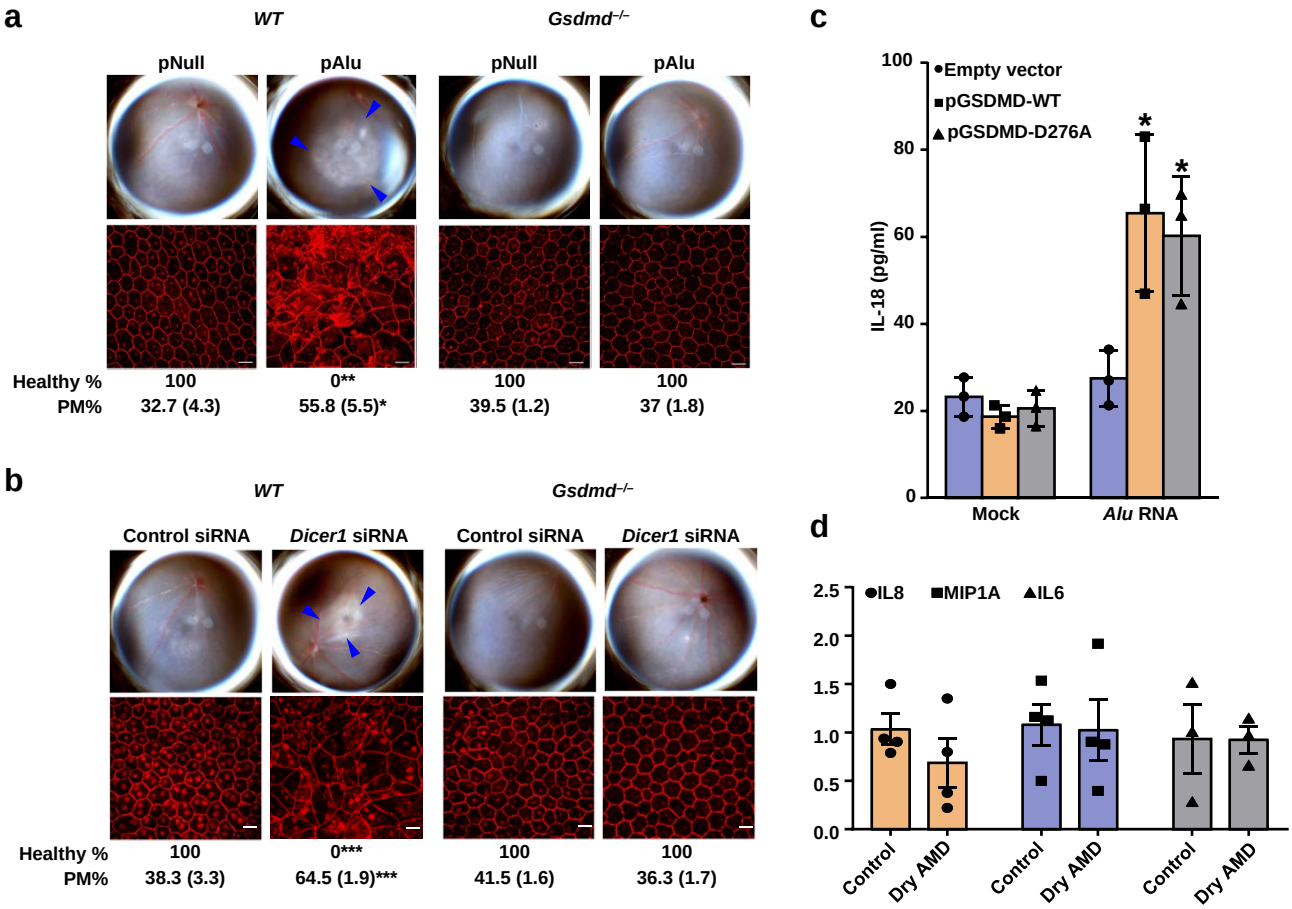

Supplementary figure 6

a

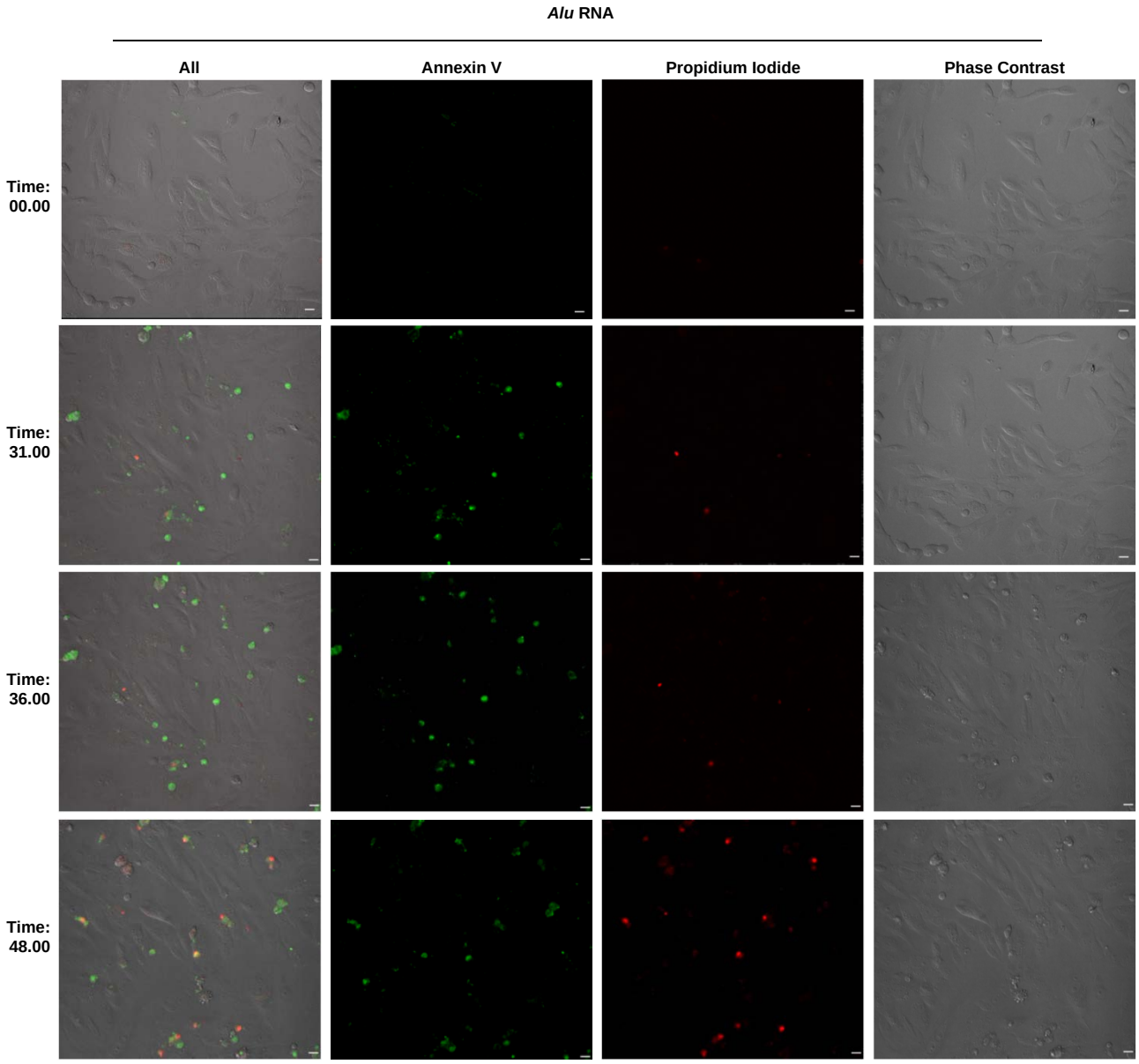

Supplementary figure 6

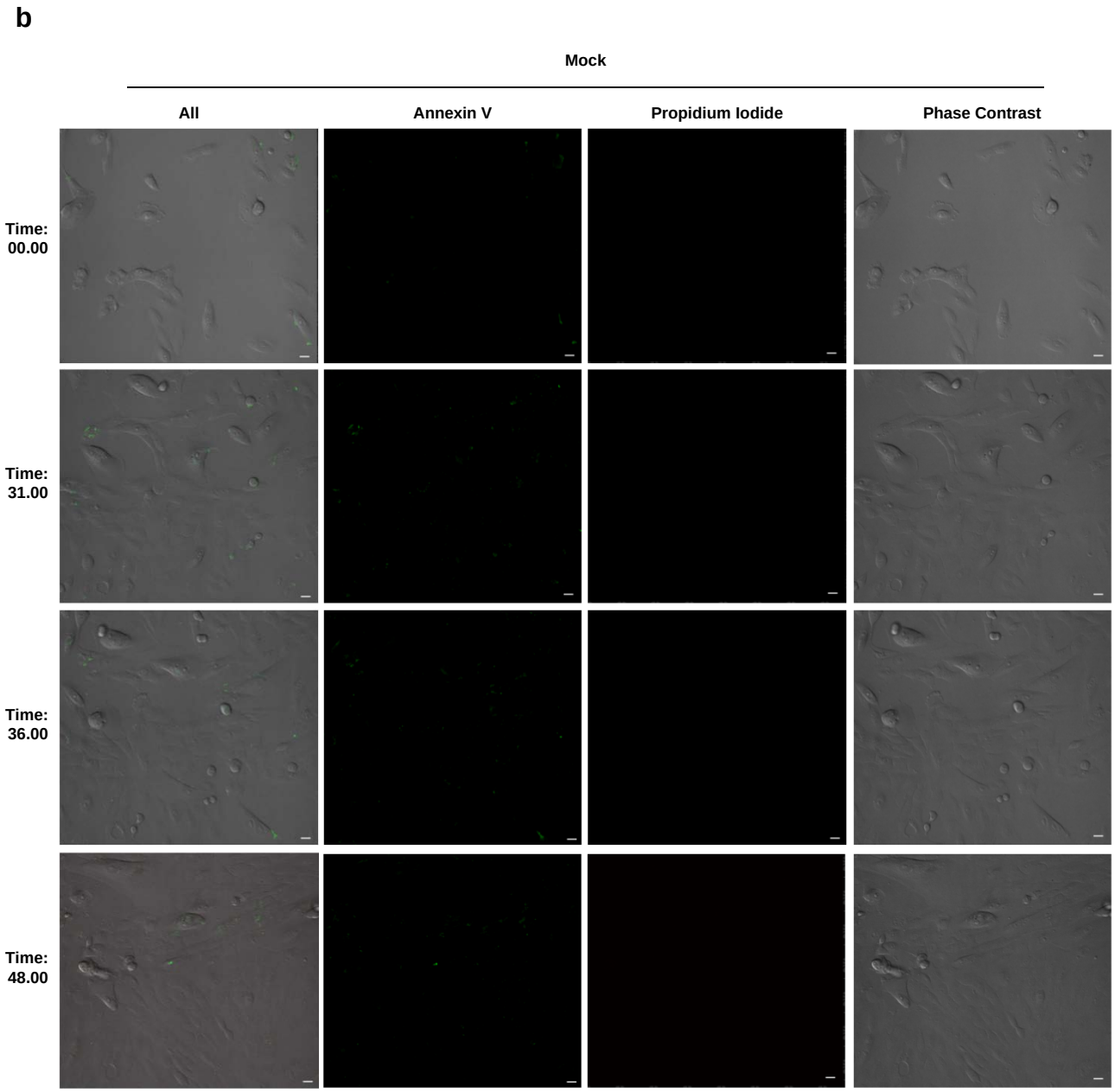

Supplementary figure 7

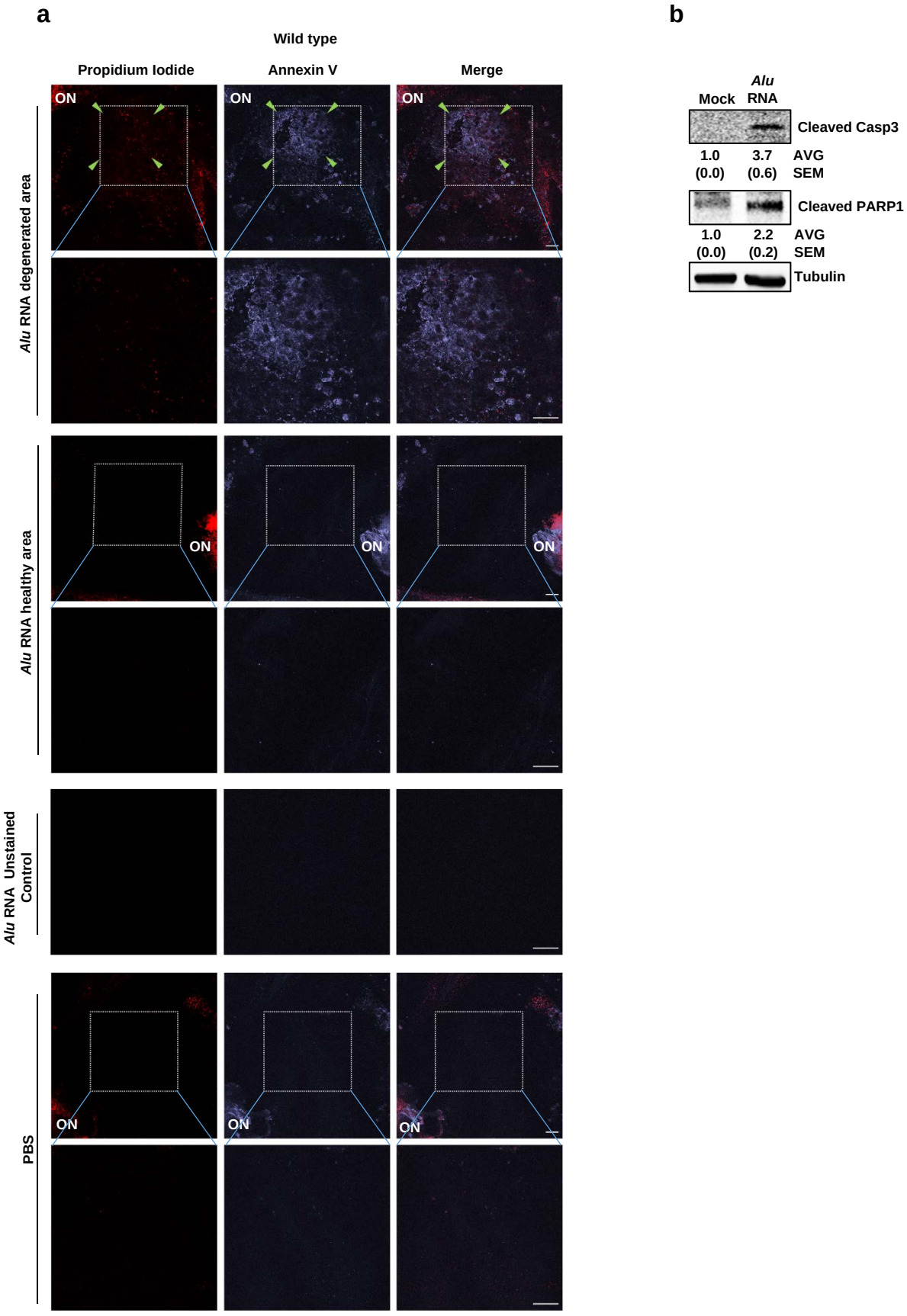

Supplementary figure 8

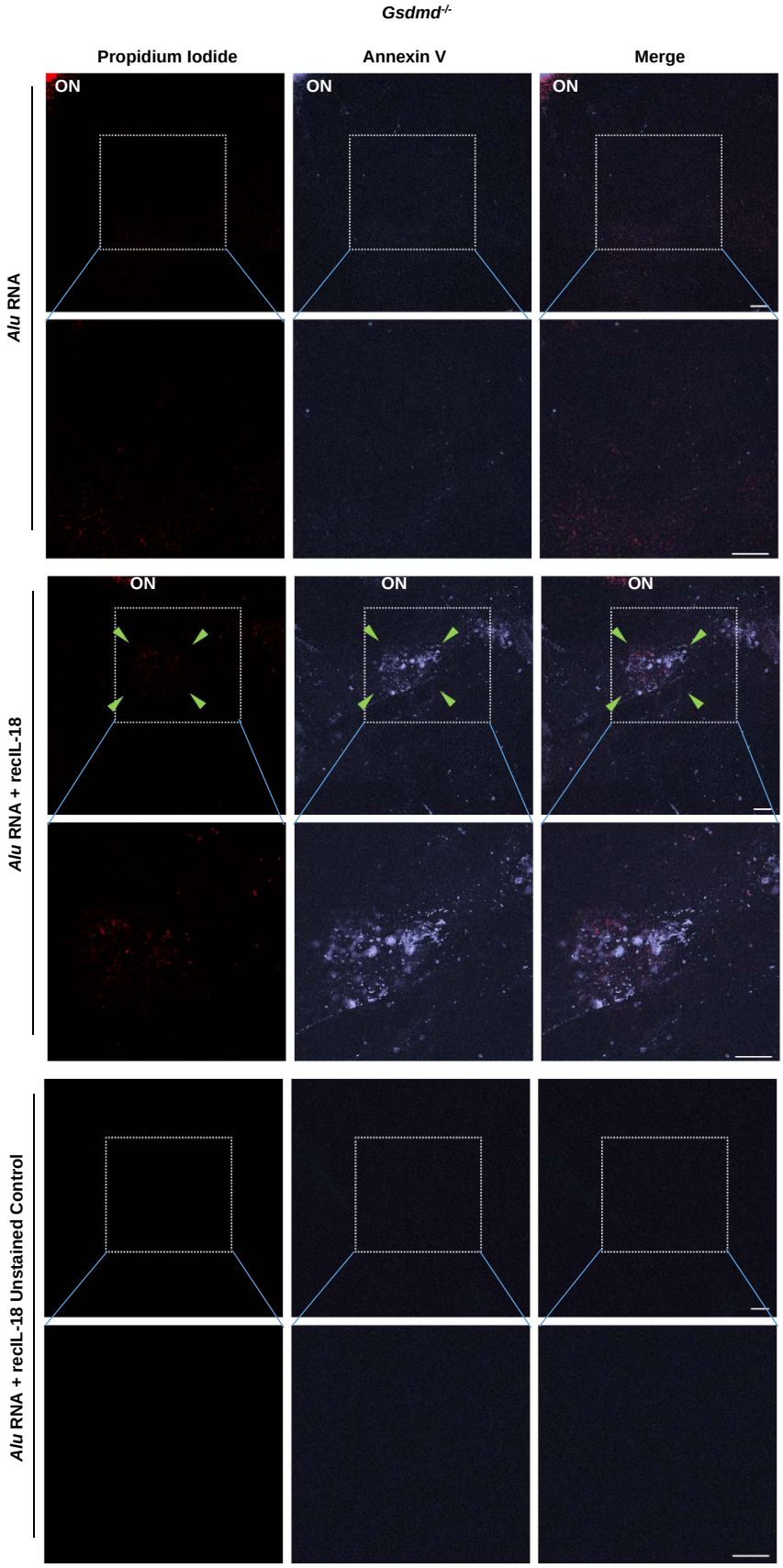

Supplementary figure 9

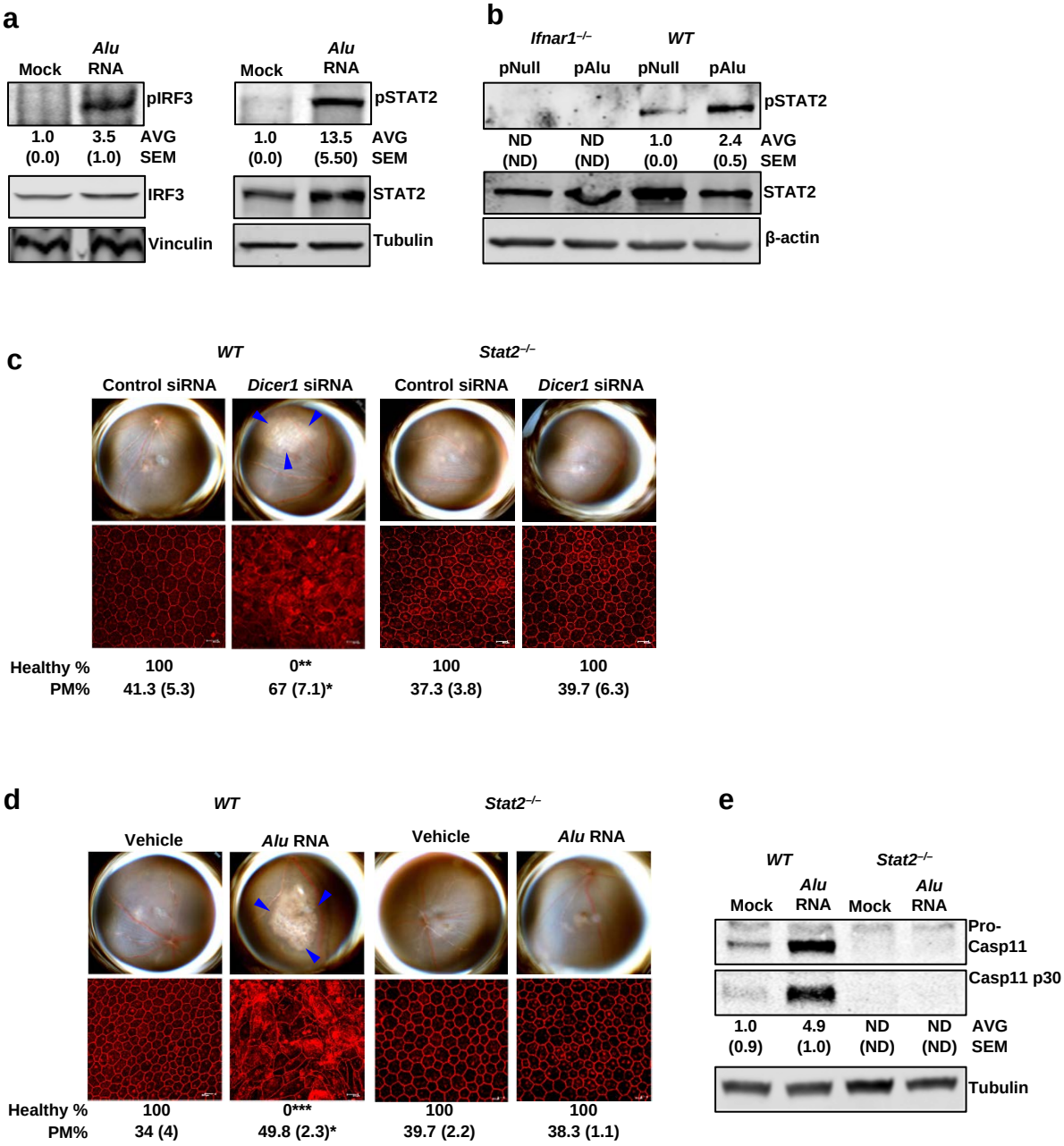

Supplementary figure 10

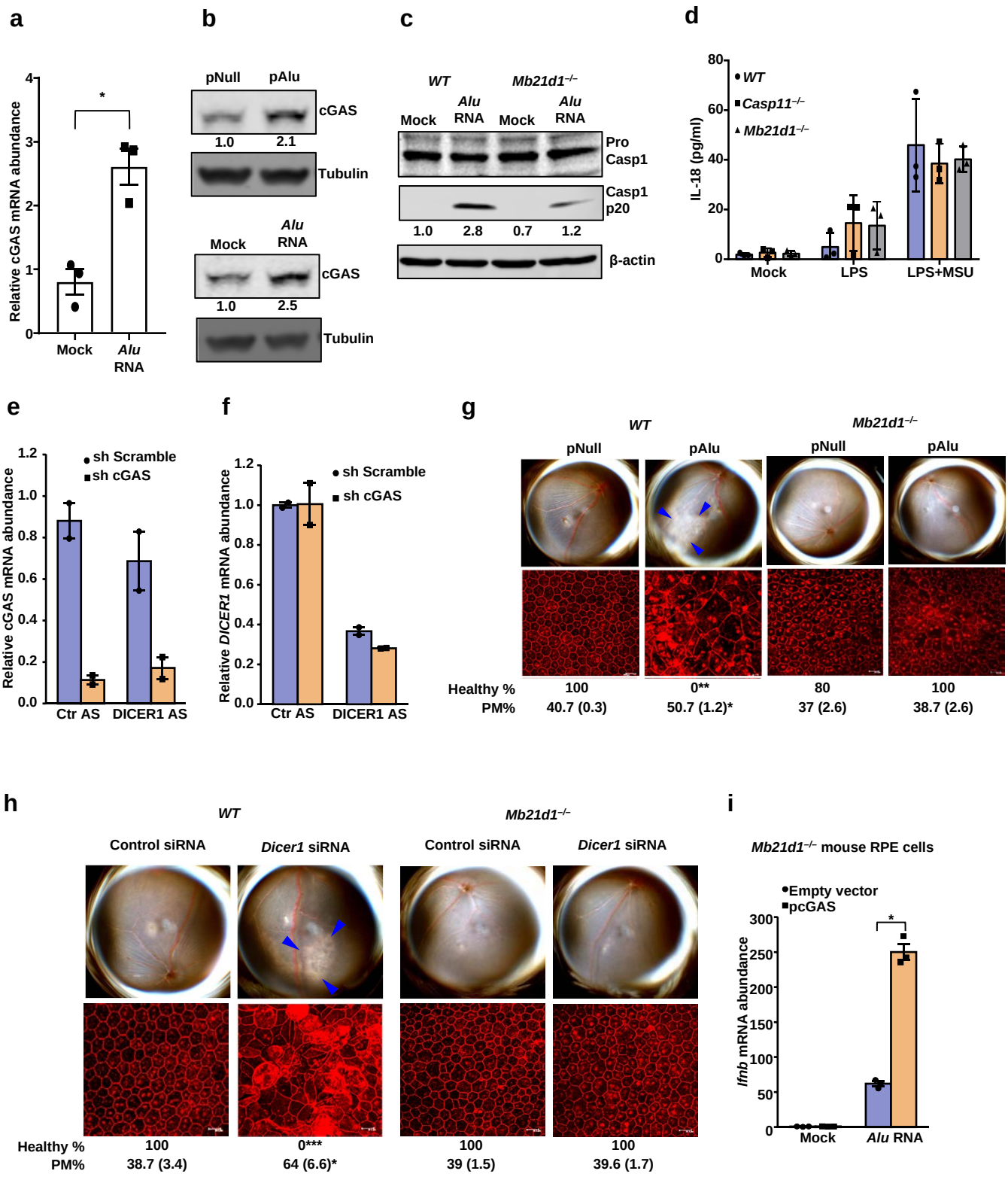

Supplementary figure 11

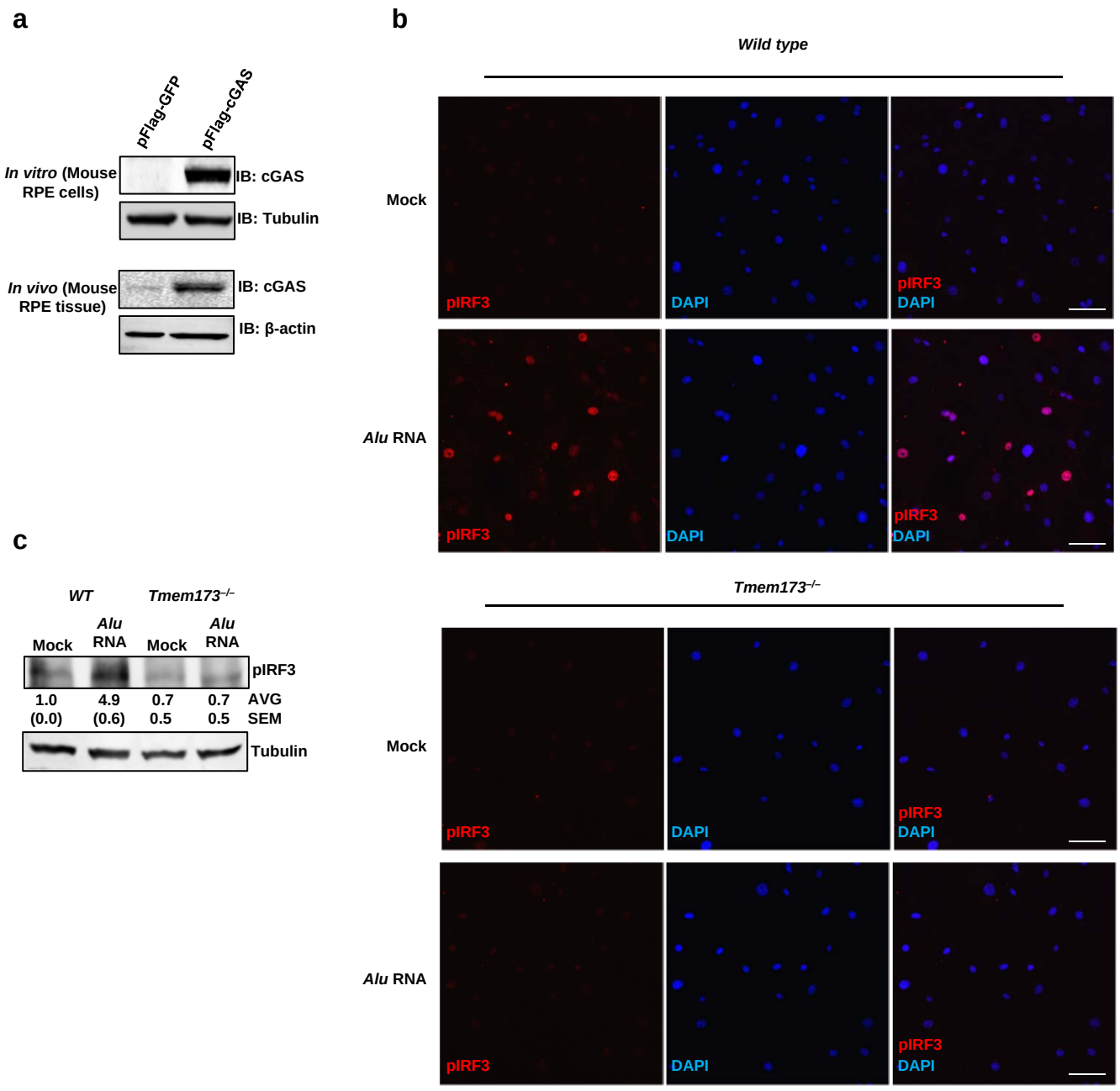

Supplementary figure 12

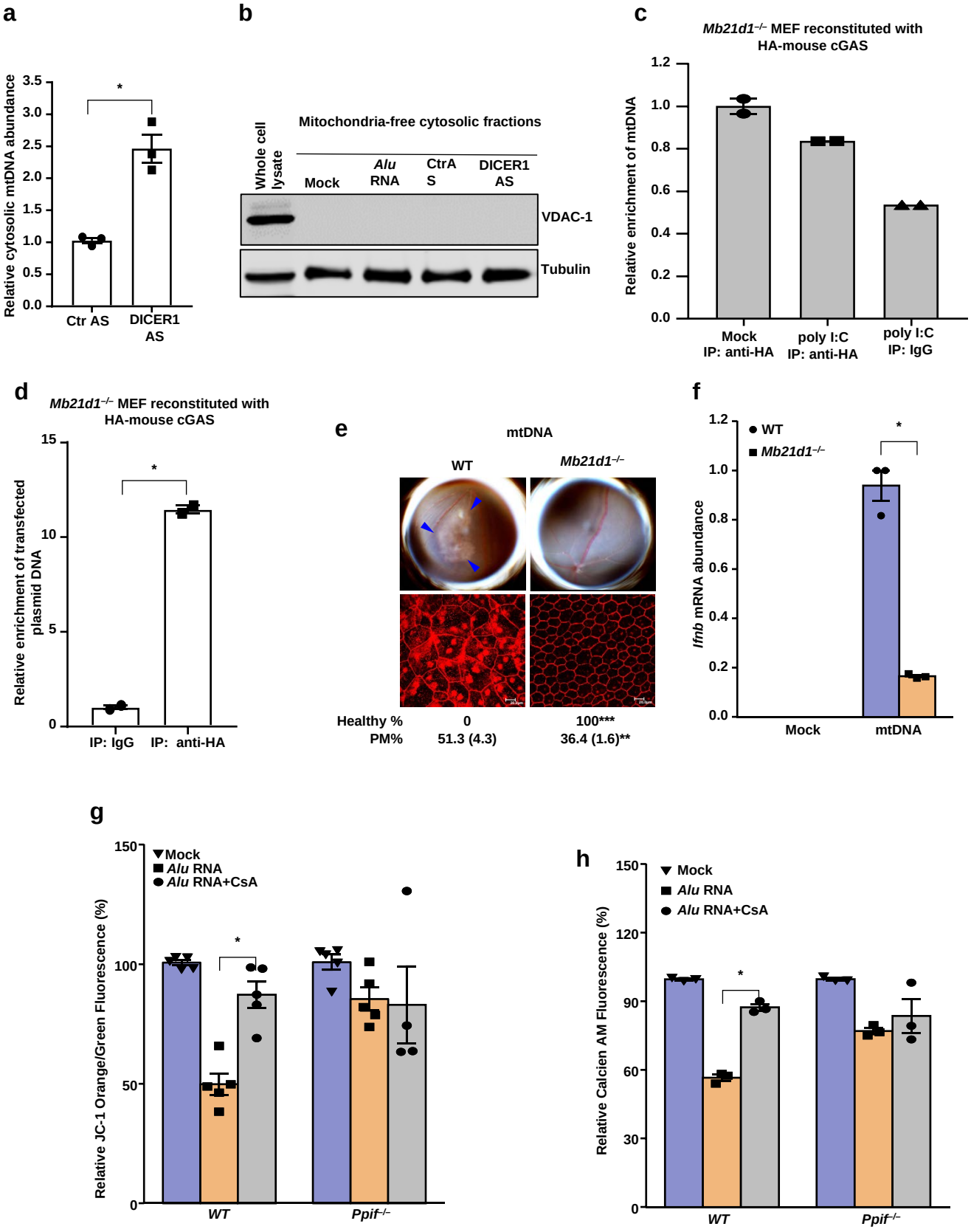

Supplementary figure 13

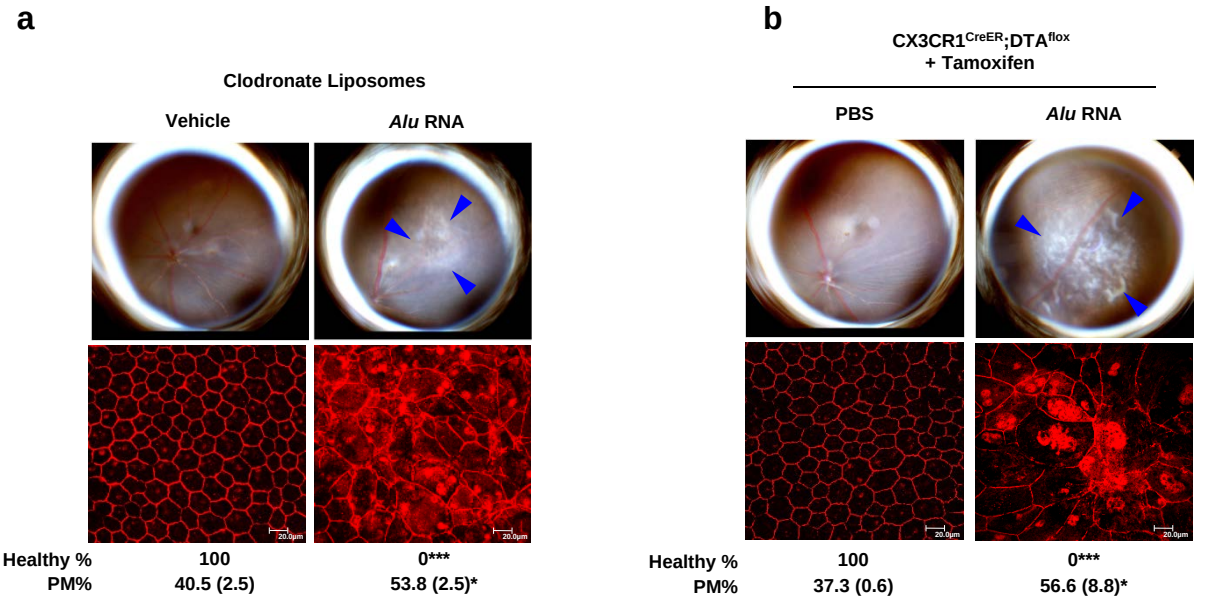

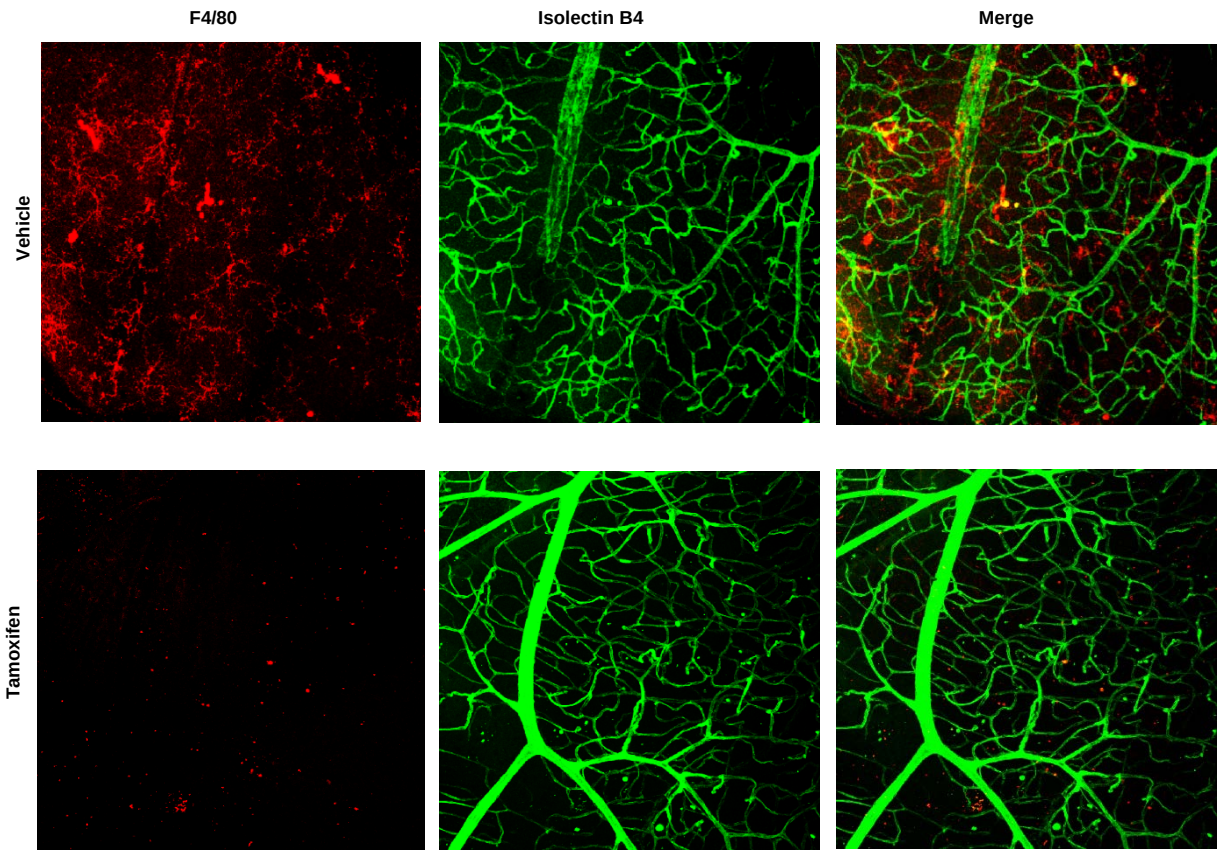

Supplementary figure 14

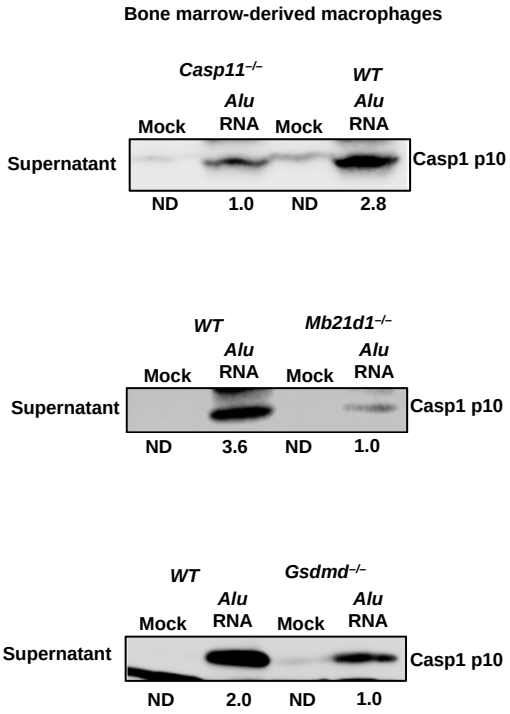

Supplementary figure 15

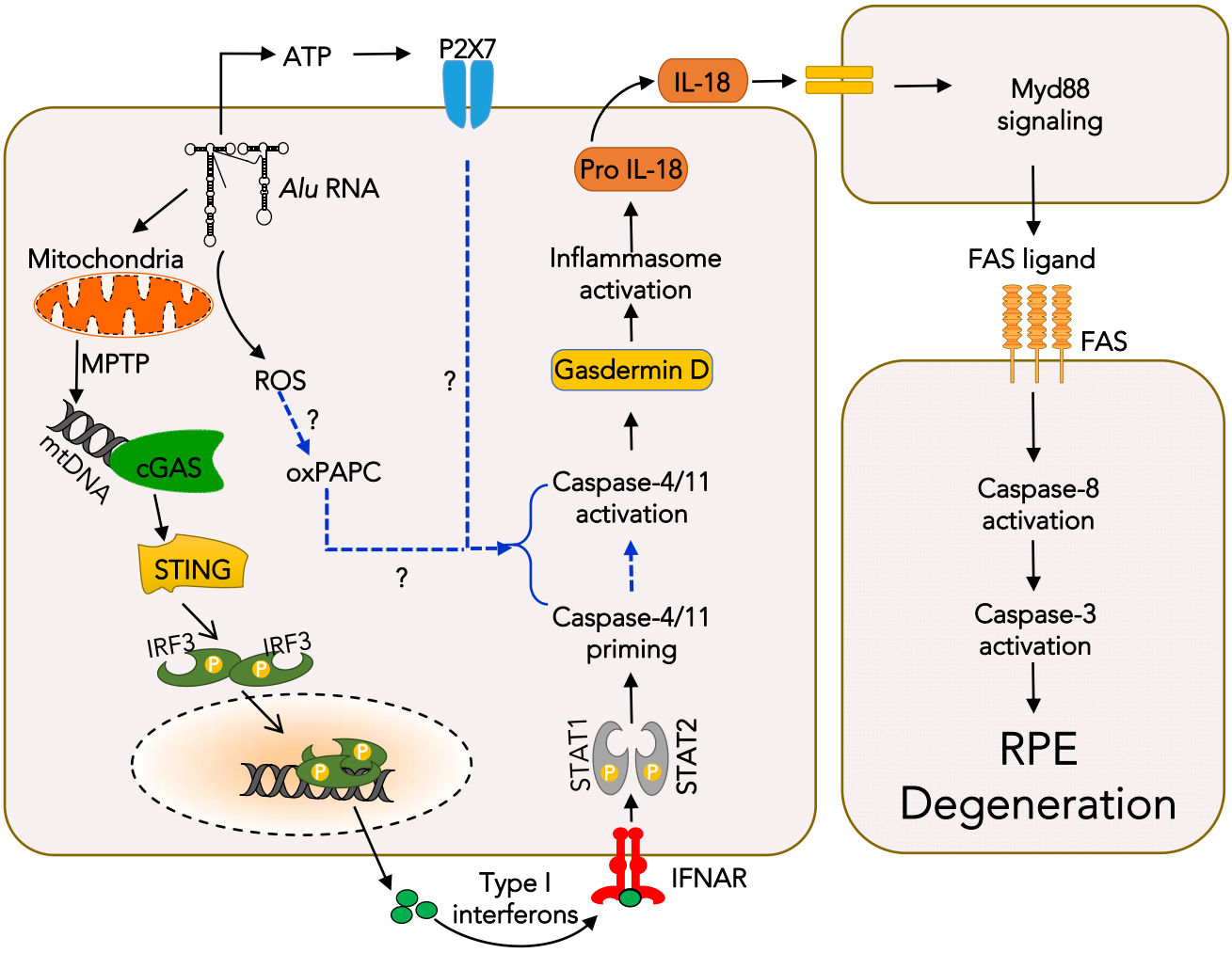

Figure 1a

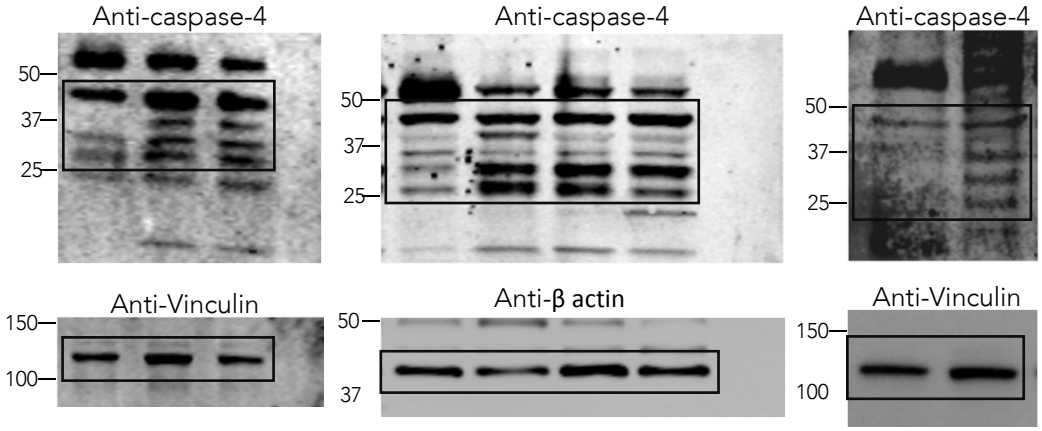

Figure 1b

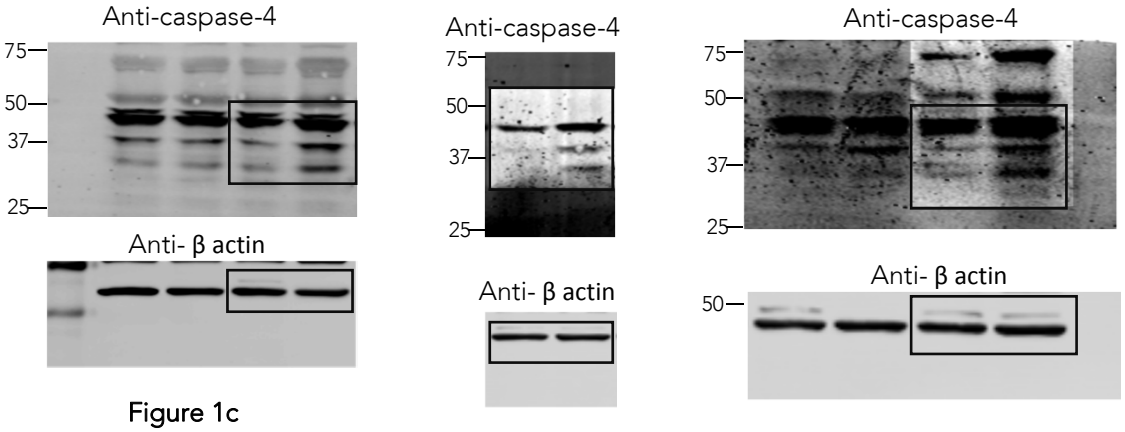

Figure 1c

Anti-caspase-11

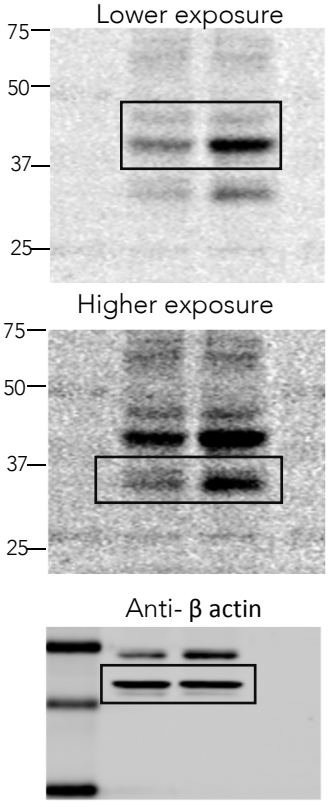

Figure 1f

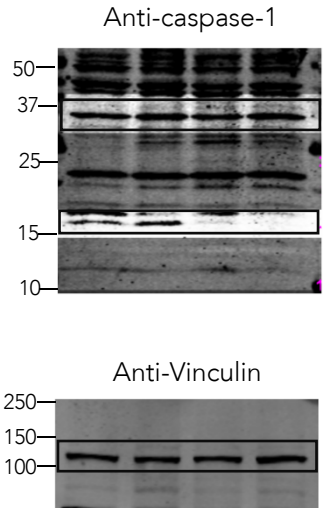

Figure 1g

Anti-caspase-1

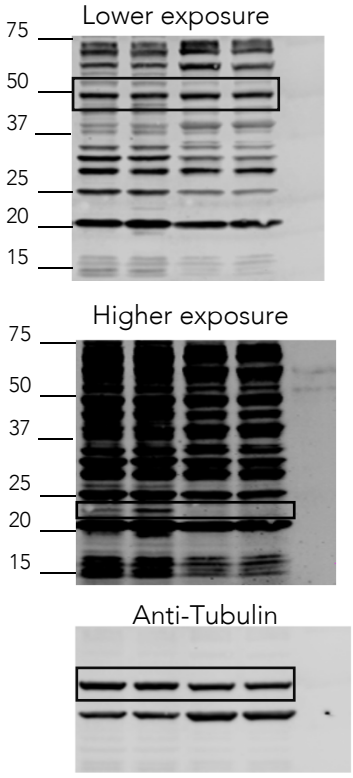

Figure 2c

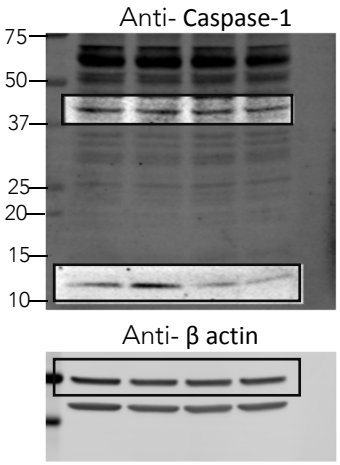

Figure 2d

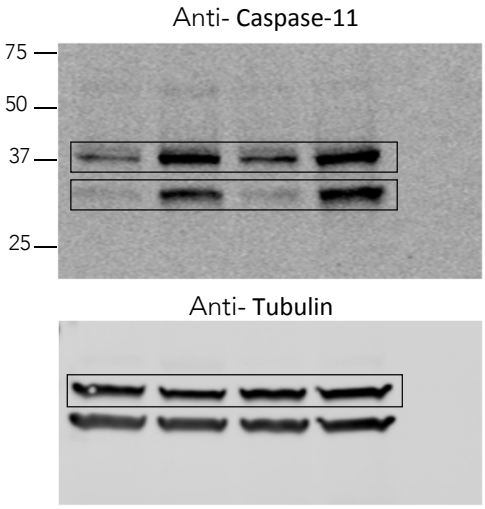

Figure 2e

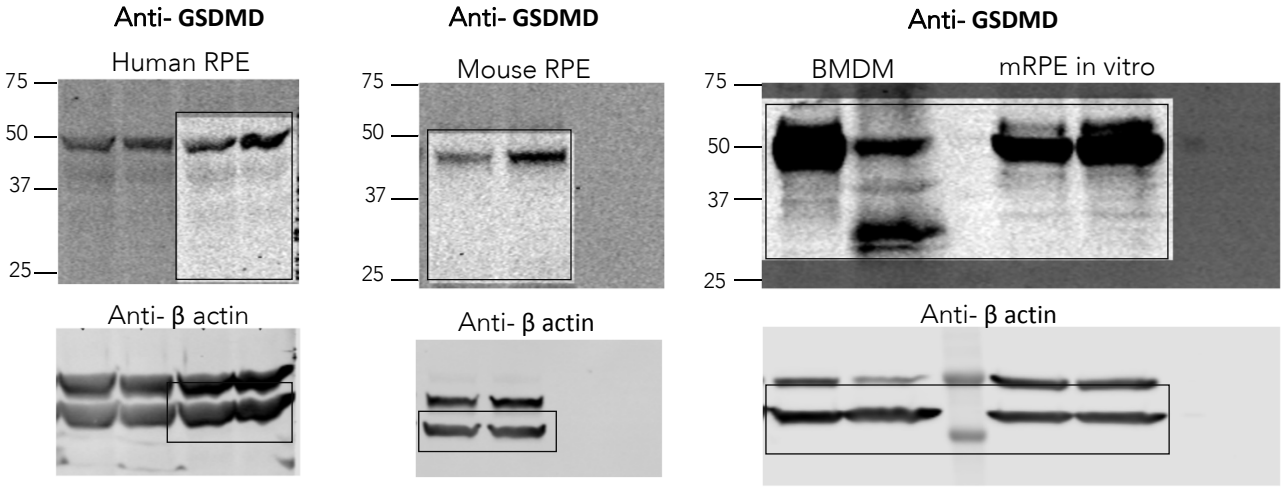

Figure 3b

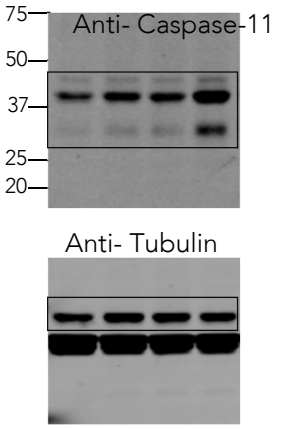

Figure 3c

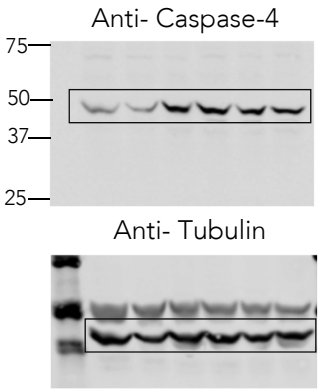

Figure 3e

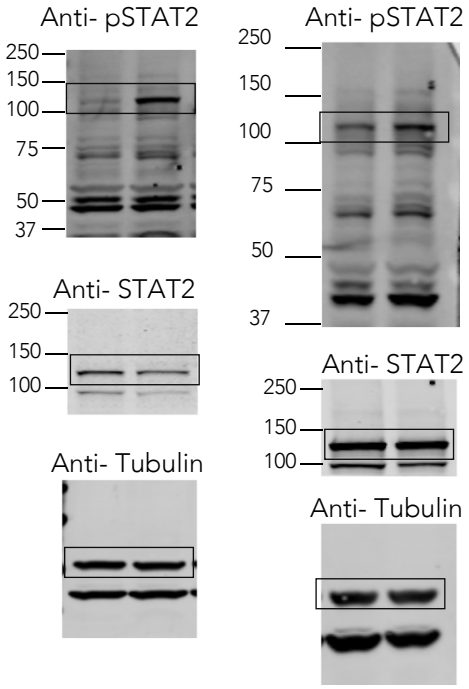

Figure 4b

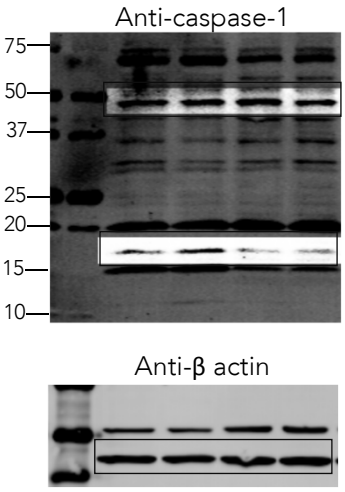

Figure 4c

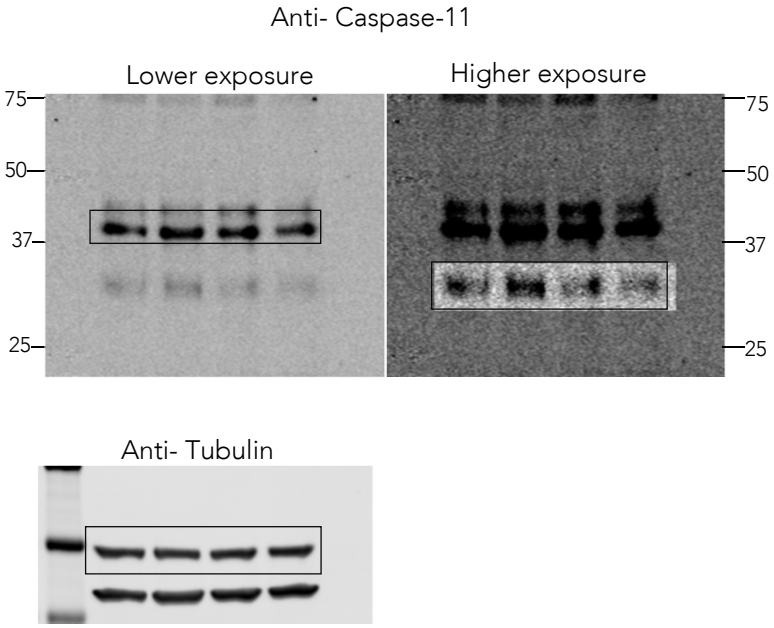

Figure 4f

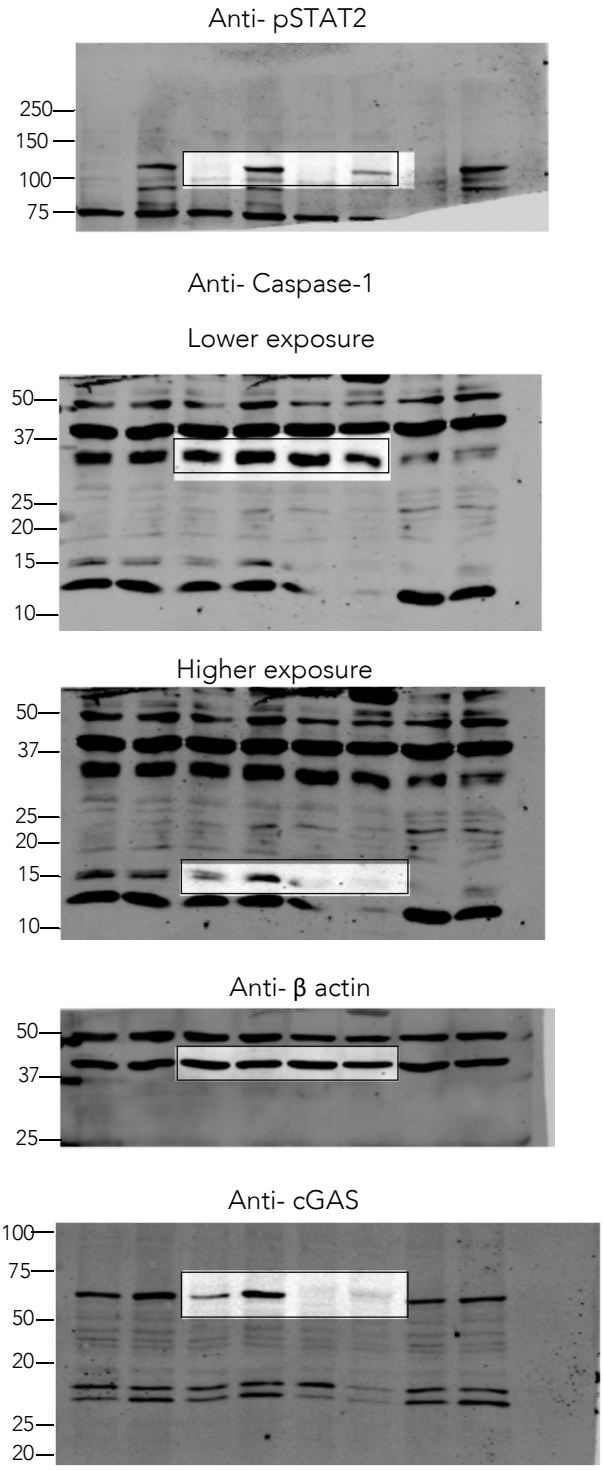
Anti- pSTAT2
250
150
100
75
Anti- Caspase-1
Lower exposure
50
37
25
20
15
10
Higher exposure
50
37
25
20
15
10
Anti- β actin
50
37
25
Anti- cGAS
100
75
50
20
25
20

Figure 5b

Anti- Caspase-1

Lower exposure

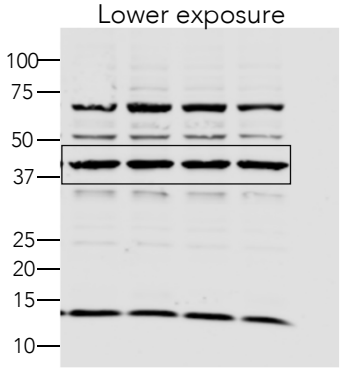

Higher exposure

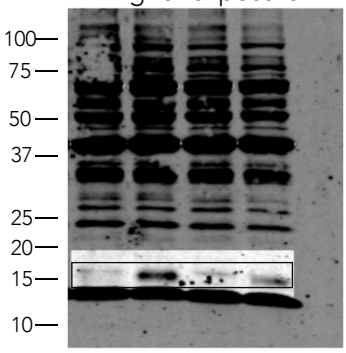

Anti- β actin

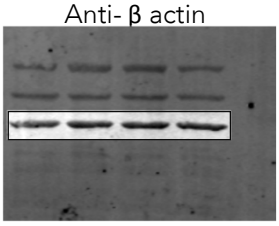

Figure 5c

Anti- Caspase-11

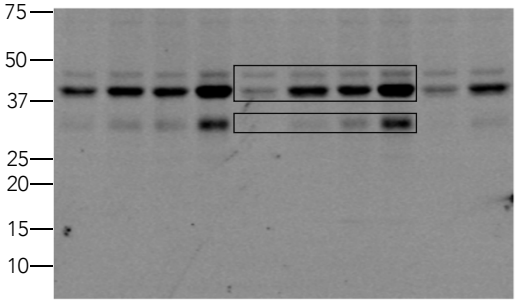

Anti- Tubulin

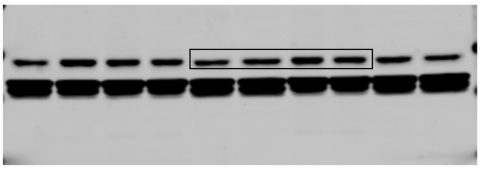

Figure 6e

Anti- Caspase-1

Lower exposure

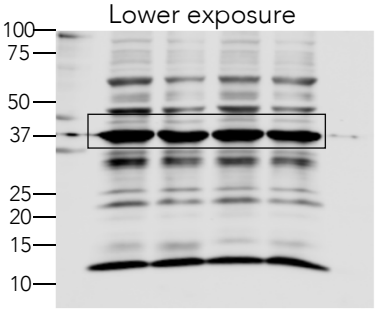

Higher exposure

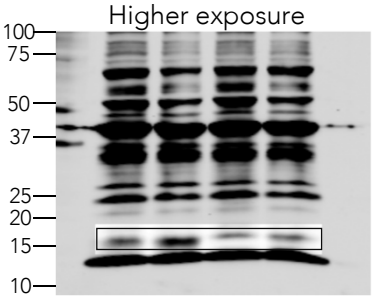

Anti- β actin

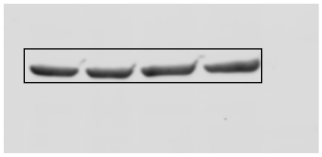

Figure 6f

Anti- Caspase-11

Lower exposure

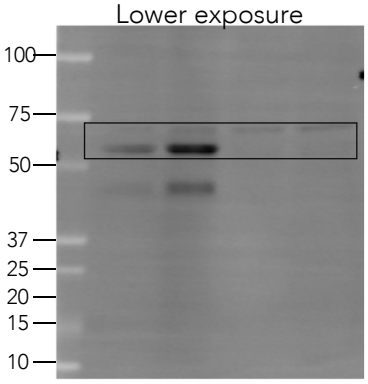

Higher exposure

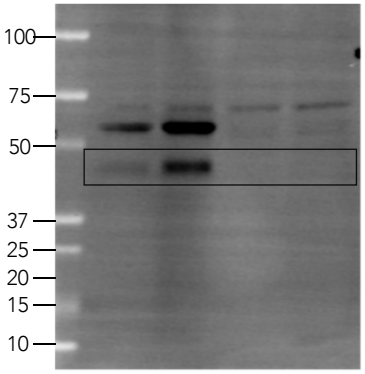

Anti- β actin

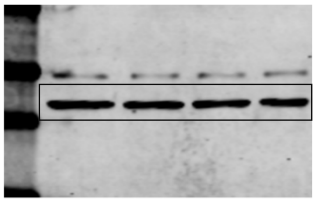

Figure 6g

Anti- Caspase-4

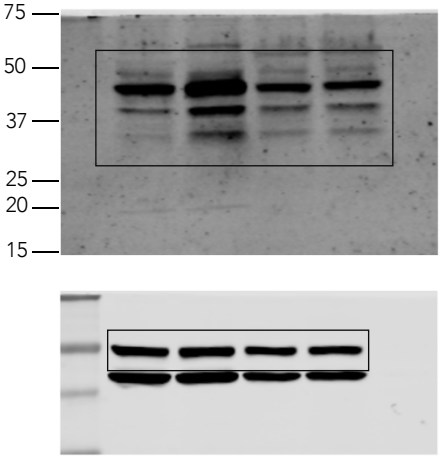

Supplementary Figure 1b

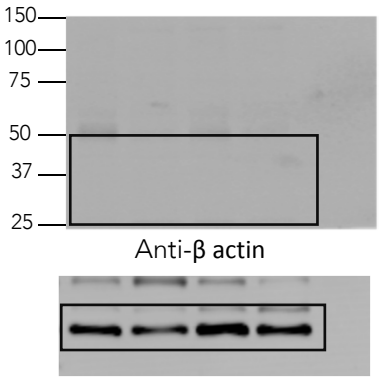

Supplementary Figure 1c

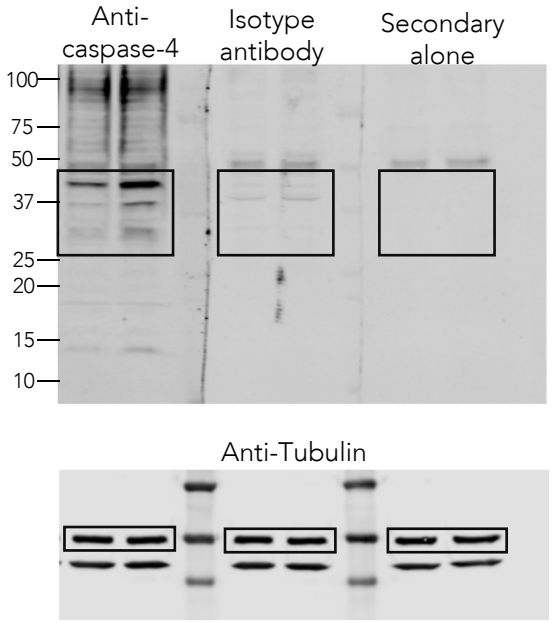

Supplementary Figure 1d

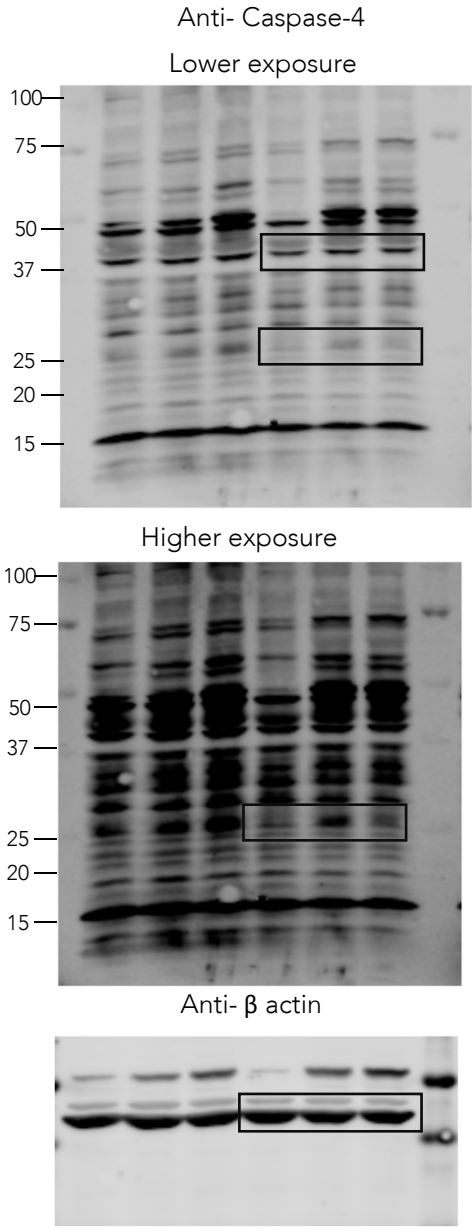

Supplementary Figure 1e

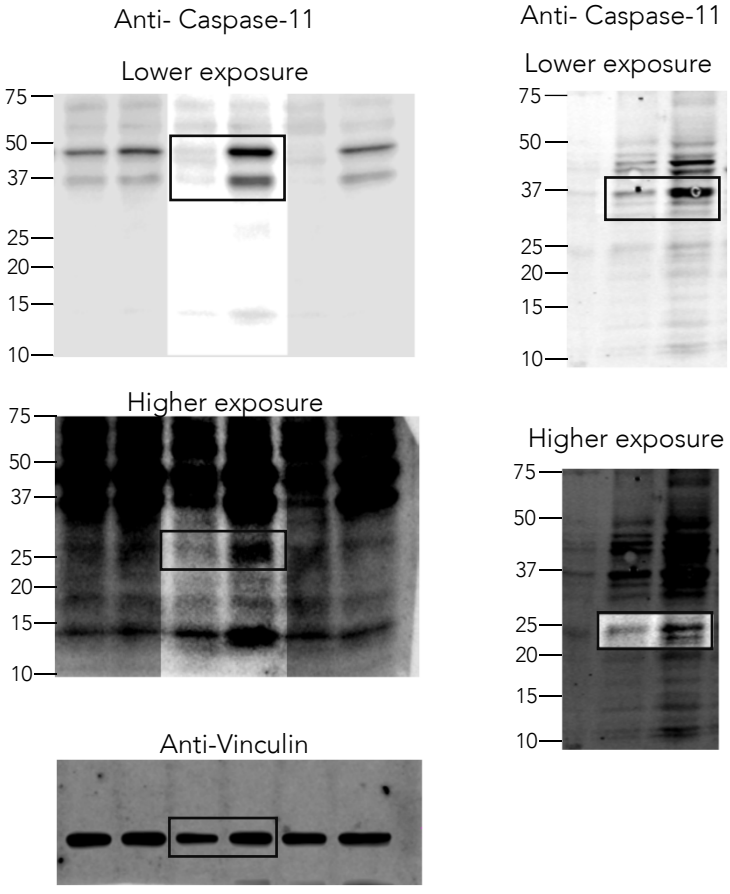

Supplementary Figure 2b

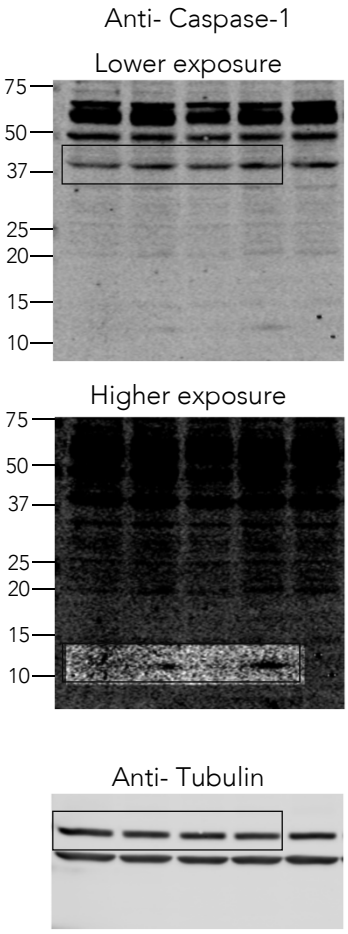

Supplementary Figure 2d

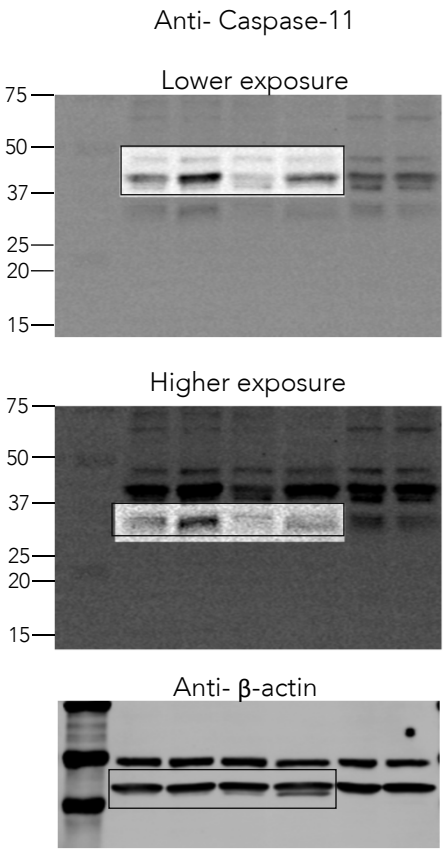

Supplementary Figure 2e

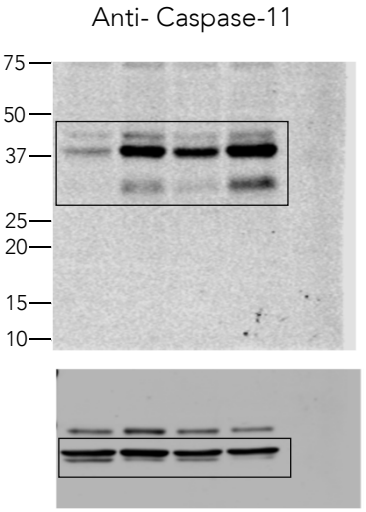

Supplementary Figure 7b

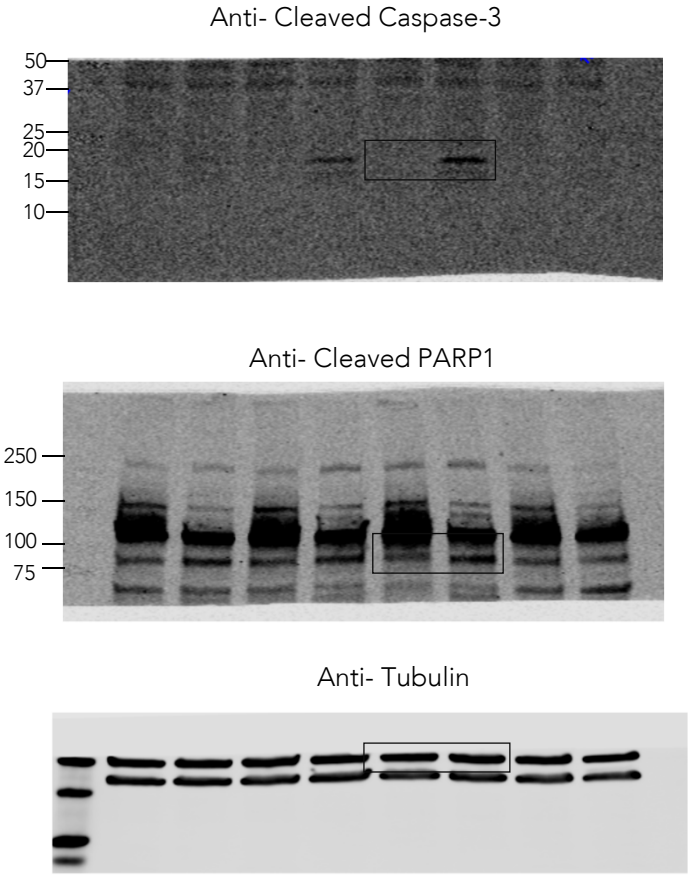

Supplementary Figure 9a

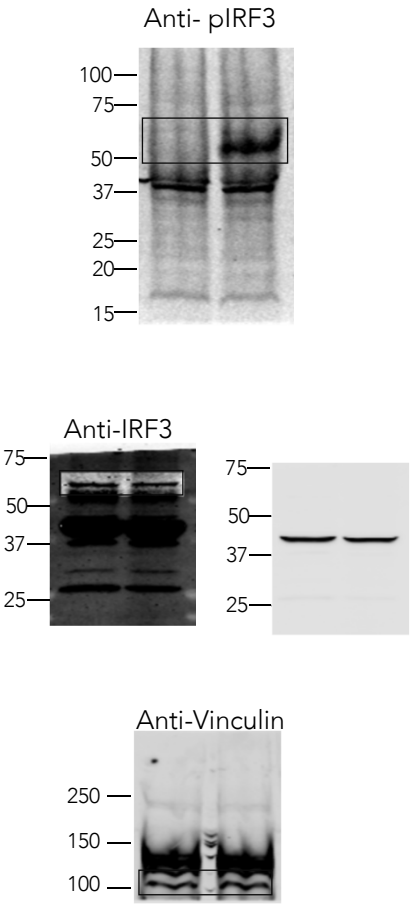

Supplementary Figure 9b

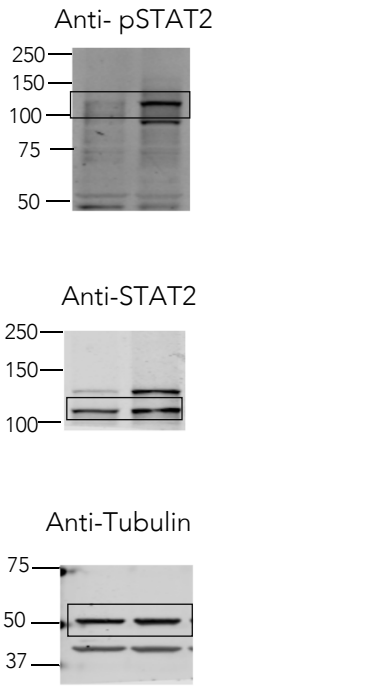

Supplementary Figure 9c

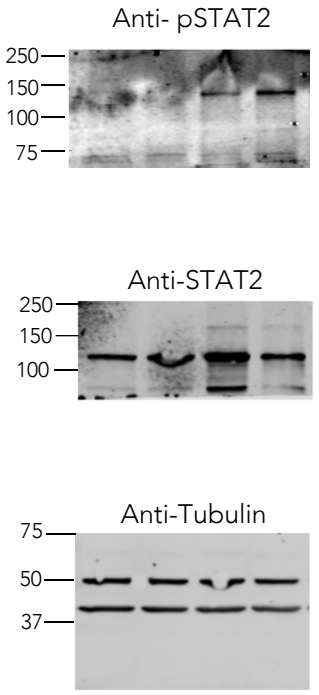

Supplementary Figure 9e

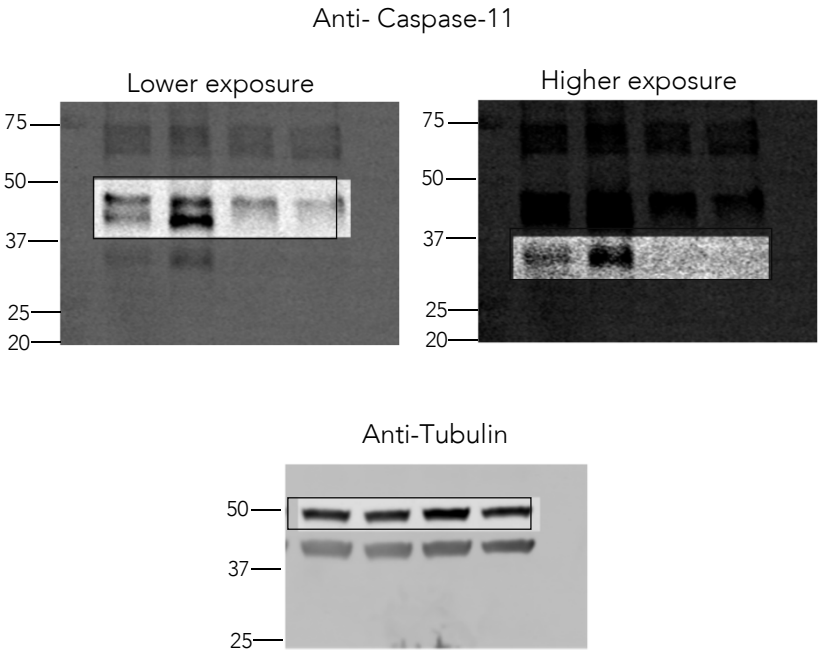

Supplementary Figure 10b

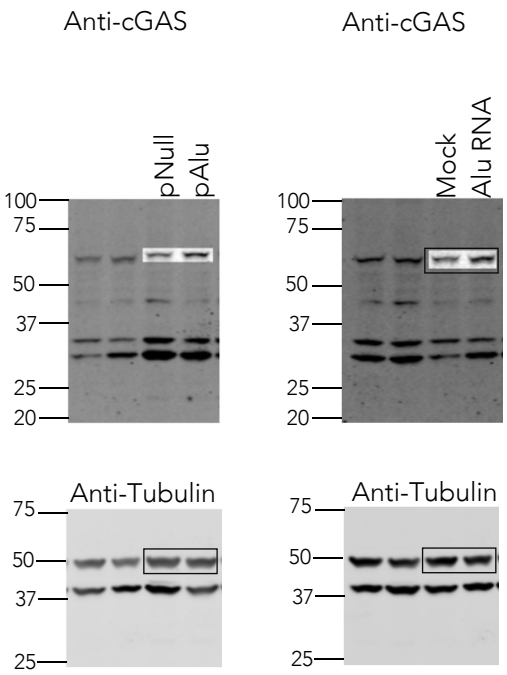

Supplementary Figure 10c

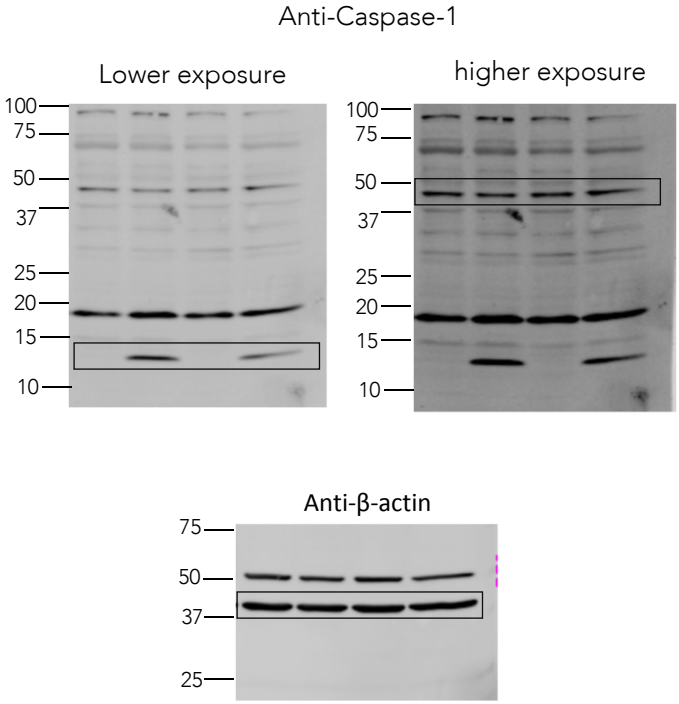

Supplementary Figure 11a

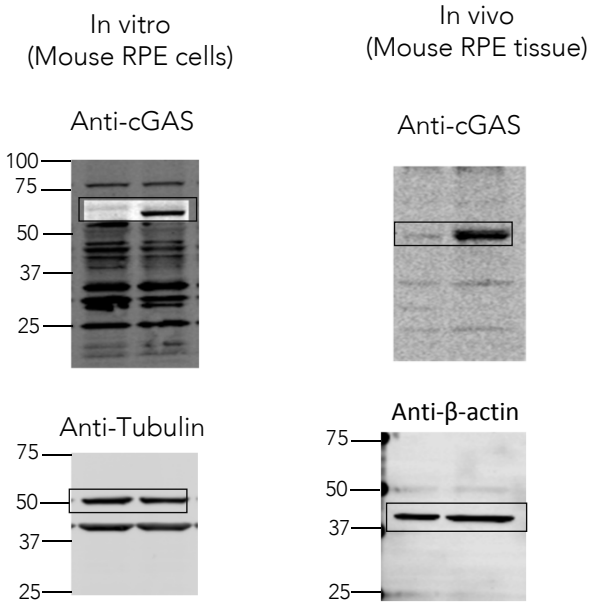

Supplementary Figure 11c

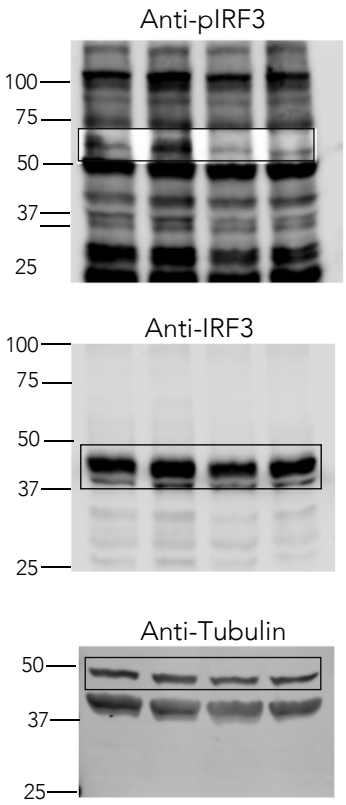

Supplementary Figure 12b

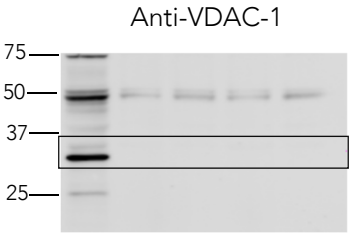

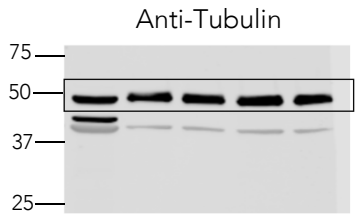

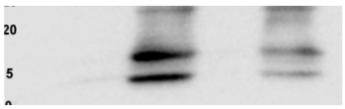

Supplementary Figure 14